Inorganic Chemistry
Cite This: Inorg. Chem. 2018, 57, 3683−3698
Article
pubs.acs.org/IC

# Magneto-Structural Properties and Theoretical Studies of a Family of Simple Heterodinuclear Phenoxide/Alkoxide Bridged $Mn^{III}Ln^{III}$ Complexes: On the Nature of the Magnetic Exchange and Magnetic Anisotropy

Mikko M. Hänninen,*[,†] Antonio J. Mota,[‡] Reijo Sillanpää,[†] Sourav Dey,[§] Gunasekaran Velmurugan,[§] Gopalan Rajaraman,*[,§] and Enrique Colacio*[,‡]

[†]Department of Chemistry, University of Jyväskylä, P.O. Box 35, FIN-40014 Jyväskylä, Finland

[‡]Departamento de Química Inorgánica, Facultad de Ciencias, Universidad de Granada, Avda. de Fuentenueva s/n, 18071 Granada, Spain

[§]Department of Chemistry, Indian Institute of Technology Bombay, Powai, Mumbai 400076, India

Supporting Information

**ABSTRACT:** A family of $Mn^{III}Ln^{III}$ strictly dinuclear complexes of general formula $[Mn^{III}(\mu\text{-L})(\mu\text{-OMe})(NO_3)Ln^{III}(NO_3)_2(MeOH)]$ ($Ln^{III}$ = Gd, Dy, Er, Ho) has been assembled in a one pot synthesis from a polydentate, multipocket aminobis(phenol)ligand [6,6′-{(2-(1-morpholyl)ethylazanediyl)bis-(methylene)}bis(2-methoxy-4-methylphenol)], $Mn(NO_3)_2{\cdot}4H_2O$, $Ln(NO_3)_3{\cdot}nH_2O$, and $NEt_3$ in MeOH. These compounds represent the first examples of fully structurally and magnetically characterized dinuclear $Mn^{III}Ln^{III}$ complexes. Single X-ray diffraction studies reveal that all complexes are isostructural, consisting of neutral dinuclear molecules where the $Mn^{III}$ and $Ln^{III}$ metal ions, which exhibit distorted octahedral $MnN_2O_4$ and distorted $LnO_9$ coordination spheres, are linked by phenoxide/methoxide double bridging groups. Static magnetic studies show that the $Mn^{III}Gd^{III}$ derivative exhibits a weak antiferromagnetic interaction between the metal ions, with a negative axial zero-field splitting $D$ parameter. The $Mn^{III}Gd^{III}$ complex shows a notable magnetocaloric effect with magnetic entropy change at 5 T and 3 K of $-\Delta S_m$ = 16.8 J $kg^{-1}$ $K^{-1}$. Theoretical studies were performed to support the sign and magnitude of the magnetic anisotropy of the $Mn^{III}$ ion (*ab initio*), to predict the value and nature of $J_{MnGd}$, to disclose the mechanism of magnetic coupling, and to establish magneto-structural correlations (DFT calculations). The results of these calculations are corroborated by quantum theory of atoms in molecule analysis (QTAIM). Finally, $Mn^{III}$−$Dy^{III}$ and $Mn^{III}$−$Er^{III}$ complexes show field-induced slow relaxation of the magnetization but without reaching a maximum above 2 K in the out-of-phase ac susceptibility. *Ab initio* calculations were also performed on $Mn^{III}$−$Dy^{III}$/$Ho^{III}$ systems to unravel the origin behind the weak SMM characteristics of the molecules possessing two strongly anisotropic ions. The mechanism of magnetic relaxation was developed, revealing a large QTM/tunnel splitting at the single-ion level. Furthermore, the anisotropy axes of the $Mn^{III}$ and $Ln^{III}$ ions were calculated to be noncollinear, leading to reduction of the overall anisotropy in the molecules. Hence, the herein reported complexes demonstrate that a combination of two anisotropic metal ions does not guarantee SMM behavior.

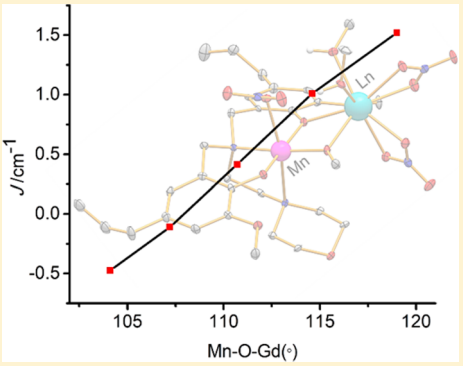


## INTRODUCTION

In recent years, heterometallic 3d/4f coordination compounds have attracted much attention not only because of the aesthetically pleasant structures they can exhibit, but also because of their interesting photophysical,[1] catalytic,[2] and magnetic properties.[3] Owing to the weak effects exerted by the ligands on the f electrons (they are very efficiently shielded by the fully occupied 5s and 5p orbitals), $Ln^{3+}$ complexes possess large orbital angular momentum and therefore a large magnetic anisotropy and magnetic moment in the ground state.[4] The exception is the $Gd^{3+}$ ion, which is largely isotropic. Bearing this in mind, researchers have tried to take advantage of these properties of the $Ln^{3+}$ ions to synthesize new 3d/4f lanthanide complexes with interesting magnetic properties. The research work has aimed not only to understand the most relevant factors governing the magnitude and sign of the magnetic coupling between 3d and 4f metal ions, but also to exploit this information to design new complexes that could ultimately behave as single molecule magnets (SMMs)[5] and as low-temperature molecular magnetic coolers (MMCs)[6] with improved properties. SMMs are molecular coordination compounds of diverse nuclearity that exhibit slow relaxation for reversal of magnetization and magnetic hysteresis below a

Received: November 15, 2017
Published: March 22, 2018






DOI: 10.1021/acs.inorgchem.7b02917
Inorg. Chem. 2018, 57, 3683−3698

blocking temperature ($T_B$). In most cases, this behavior is tied to the existence of a thermal energy barrier ($U$), which primarily depends on the magnetic anisotropy, that prevents the reversal of the molecular magnetization when the polarizing field is removed, leading to magnetic bistability below $T_B$. These nanomagnets present attractive future applications in fields of molecular spintronics,[7] ultra-high-density magnetic information storage,[8] and quantum computing at the molecular level.[9]

A large number of 3d/4f complexes have been reported, and some of them indeed show an SMM behavior.[3] Nevertheless, most of these SMMs have been demonstrated to exhibit only small or even negligible energy barriers. This has been attributed to (i) a subtractive combination of the local anisotropies, resulting in a small anisotropy for the whole molecule, and (ii) a small gap between the low-lying energy sublevels, resulting from weak magnetic exchange interaction between 3d and 4f metal ions, which allows mixing of low-lying excited states in the ground state. This wave function mixture favors quantum tunnelling of magnetization (QTM), thus reducing the thermal energy barrier to a small effective value. Recent experimental and theoretical studies have shown that the magnitude of the magnetization relaxation barrier depends on both single-ion anisotropy and 3d/4f magnetic exchange interactions.[10] Thus, when the 3d/4f magnetic exchange coupling is strong enough, the exchange coupled levels are well-separated (avoiding mixing of low-lying excited states in the ground state), and the QTM is suppressed, so that large energy barriers, hysteresis loops, and relaxation times are observed.

It is important to notice that only a few heterometallic 3d/4f complexes, where the magnetic exchange interaction can effectively reduce the QTM process, have been reported so far. The best example of this phenomenon is the family of heterometallic tetranuclear $Cr^{III}_2$ $Ln^{III}_2$ butterfly-like complexes recently reported by Murray et al.,[10b,f,11] which present strong magnetic exchange interactions ($J_{Cr-Dy}$ = 7−10 $cm^{-1}$). They have demonstrated that the magnetic relaxation dynamics can be either positively or negatively biased by varying the main amine−polyalcohol ligand, as well as the ancillary bidentate bridging ligands connecting $Cr^{III}$ and $Ln^{III}$ ions.[10b] This is because the variation in these ligands affects the magnetic exchange interactions between metal ions and their magnetic anisotropy. Moreover, they have also shown that $Tb^{III}$ and $Ho^{III}$ counterparts can also exhibit SMM behavior with highly coercive hysteresis loops and long relaxation times.[10b] In view of the central role played by 3d/4f magnetic exchange interactions in the SMMs, there exists great interest in synthesizing and magneto-structurally characterizing simple complexes with a small number of 3d and 4f ions, preferably dinuclear complexes, to establish accurate magneto-structural correlations and to use them to better understand the relationship between the SMM behavior and the exchange interactions. This information is crucial for designing new 3d/4f complexes with improved SMM properties. It is worth noting that some examples of simple dinuclear $M^{II}$−$Ln^{III}$ SMMs ($M^{II}$ = Cu, Ni, Co)[3] have been reported so far, and theoretical and experimental magneto-structural correlations have been established for the $M^{II}$−$Gd^{III}$ counterparts ($M^{II}$ = Cu, Ni).[12] However, as far as we know, no examples of structurally characterized dinuclear $Mn^{III}Gd^{III}$ complexes exist, and consequently, no magneto-structural correlation have been established for them.

MMCs are complexes exhibiting an enhanced magnetocaloric effect (MCE), which is based on the change of magnetic entropy upon application of a magnetic field and can be exploited for molecular refrigeration.[6] Contrary to SMM behavior, which is favored by highly anisotropic $Ln^{3+}$ ions, the MCE is improved in molecules containing isotropic metal ions and exhibiting weak magnetic coupling between them. This is because in these conditions multiple low-lying excited, field-accessible states are generated, which can contribute to the magnetic entropy of the system. In view of the above considerations, 3d/4f dinuclear complexes containing the isotropic $Gd^{3+}$ ion, which has the maximum entropy value calculated as $R\ln(2S_{Gd} + 1)/M_{Gd}$ = 110 J $kg^{-1}$ $K^{-1}$ and the $Mn^{III}$ ion (despite being anisotropic has a maximum entropy value of 271 J $kg^{-1}$ $K^{-1}$), could be good candidates for constructing magnetic coolers.

Interestingly, even though numerous $Mn^{III}/Ln^{III}$ cluster complexes exist,[13] to the best of our knowledge, no examples of fully structurally and magnetically characterized simple dinuclear $Mn^{III}Ln^{III}$ complexes have been reported so far (an example of dinuclear $Mn^{III}Gd^{III}$ can be found in the literature, but its crystal structure was not reported).[13p] This is rather surprising, taking into account that the combination of two exchanged coupled anisotropic metal ions (octahedral $Mn^{III}$ complexes are known to exhibit significant ZFS magnetic anisotropy promoted by Jahn−Teller distortion) could represent a good strategy to design new 3d/4f SMMs. Moreover, for the most part of the magneto-structurally characterized $Mn^{III}Gd^{III}$ complexes, the magnetic exchange coupling constant $J_{MnGd}$ has not been determined due to the complexity of the system with several $Mn^{III}$−$Mn^{III}$, $Gd^{III}$−$Gd^{III}$, and $Mn^{III}$−$Gd^{III}$ interactions, where the first is by far the dominant interaction. In the remaining few cases, $J_{MnGd}$ has been reported to be very weak and either ferro- or antiferromagnetic in nature. As the $J_{MnGd}$ is the only one present in a simple dinuclear $Mn^{III}Gd^{III}$, such a compound will be the better candidate to disclose the nature of the interaction between these metal ions.

To synthesize simple dinuclear $Mn^{III}Ln^{III}$ complexes, ligands with specific binding sites allow both the preferential coordination to transition or lanthanide metal ions and the control of the nuclearity. In this regard, we have used a multidentate aminobis(phenol) ligand ($H_2L$, Figure 1), which is adapted for the formation of 3d/4f systems. In this contribution we report the synthesis, structures, magnetic properties, and computational studies of dinuclear 3d/4f $Mn^{III}Ln^{III}$ complexes of general formula $[Mn^{III}(\mu\text{-}L)(\mu\text{-}OMe)(NO_3)\text{-}Ln^{III}(NO_3)_2(MeOH)]$ ($Ln^{III}$ = Gd, Dy, Er, Ho). The aim of this work is 4-fold: (i) to establish theoretical magneto-structural correlations using the simple $Mn^{III}Gd^{III}$ dinuclear complex as model, (ii) to disclose the mechanism of exchange coupling in this complex, (iii) to analyze its magneto-thermal properties, and (iv) to examine if the large anisotropy of the $Ln^{III}$ ions, together with the coupling to the anisotropic $Mn^{III}$ ion, could lead to SMM behavior.

## RESULTS AND DISCUSSION

**Synthetic Procedures.** The ligand $H_2L$ was prepared in excellent yield using the literature procedure.[14] Complexes **1**−**4** were synthesized with good yields (51−66%) in aerobic conditions using neutral ligands and hydrated metal nitrates (Figure 1) as starting materials. As expected, prepared complexes show very good stability against air and moisture.



DOI: 10.1021/acs.inorgchem.7b02917
Inorg. Chem. 2018, 57, 3683−3698

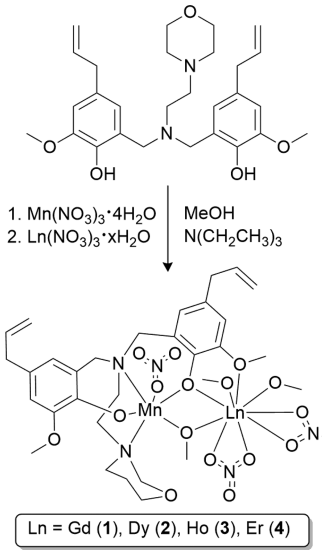


**Figure 1.** Structure of the ligand and synthetic procedure to obtain complexes **1**−**4**.

The complexes were isolated by crystallization from the reaction mixture and could be used in further analyses without any additional purification steps.

**X-ray Crystallography.** The solid-state geometries of all four complexes appear to be isostructural. Nonetheless, to be able to quantify the effects of the small changes of the geometrical parameters around the metal cations, we have determined the solid-state structures of all complexes by single crystal X-ray crystallography. Compounds **1**−**4** crystallize in the monoclinic, noncentrosymmetric *Pn* space group. The structure of **1** is depicted in Figure 2 as an example, and the selected

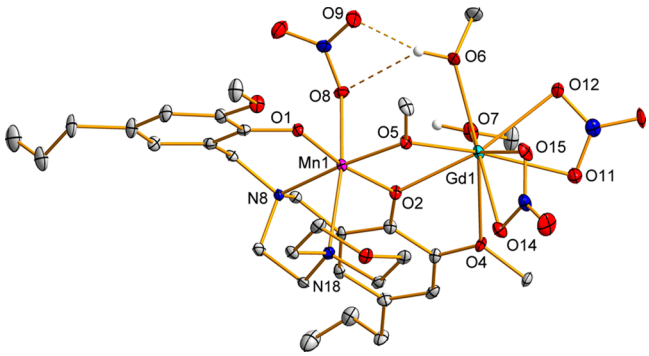


**Figure 2.** Molecular structure of **1**. C−H hydrogens are omitted for clarity, and thermal ellipsoids have been drawn at the 30% probability level.

bond lengths and angles for **1**−**4** are presented in Table 1. The structure consists of dinuclear neutral molecules, in which metal ions are linked by phenoxide/methoxide double bridging groups. The $MnN_2O_4$ distorted elongated octahedral coordination sphere around the manganese(III) cation is made of four oxygen atoms belonging to bridging and terminal phenoxide groups of the $L^{2-}$ ligand, to the methoxide bridging group and to one monocoordinated nitrate anion, and two amino nitrogen atoms pertaining to the ligand $L^{2-}$. The lanthanide ions in all complexes **1**−**4** bear a similar coordination environment, which is built by the same bridging oxygen atoms as in Mn(III), one weakly coordinated methoxy oxygen atom from aromatic substituent, four oxygen atoms from bidentate nitrate anions, and two oxygen atoms coming from two coordinated methanol molecules, thus producing a $LnO_9$ coordination sphere.

In general, the differences in the bond distances between different $Ln^{III}$ cations are minor, and deviations in bridging Mn−O−Ln angles are also quite small. The intramolecular metal−metal separation is relatively long (3.459−3.428 Å) and does not change a lot when moving from left to right in the lanthanide series. The alkoxide/phenoxide bridge is very symmetrical which indicates that the coordinating oxygen atoms are quite similar in nature.

The complexes **1**−**4** are packed as single molecules without any solvent of crystallization. However, coordinated, neutral methanol molecules form relatively strong inter- and intramolecular hydrogen bonds to the morpholine oxygen of the neighboring molecule (OH···O distance of 2.67−2.69 Å) and to the coordinated nitrate anion (OH···O distance of 2.69−3.04 Å), respectively (Figure 3). The shortest intermolecular metal−metal distance is over 8.5 Å without any clear path for magnetic interaction; hence, the observed magnetic behavior is presumably of molecular origin.

**Magnetic Properties of $[Mn^{III}(\mu\text{-L})(\mu\text{-OMe})(NO_3)\text{-}Gd^{III}(NO_3)_2(MeOH)]$ (1).** The temperature dependence of $\chi_M T$ for complexes **1**−**4** ($\chi_M$ is the molar magnetic susceptibility per $Mn^{III}Ln^{III}$ unit) in the temperature range 300−2 K range was measured with an applied magnetic field of 1000 Oe and is displayed in Figure 4 for complex **1** and in Figure 14 for complexes **2**−**4**.

We start with the simple case by studying the $Mn^{III}$−$Gd^{III}$ complex **1**. At room temperature, the $\chi_M T$ value of 11.40 $cm^3$ $mol^{-1}$ K is larger, but still close to what is expected for noninteracting $Mn^{III}$ ($S = 2$) and $Gd^{III}$ ($S = 7/2$) ions (10.875 $cm^3$ $mol^{-1}$ K with $g = 2$). On lowering the temperature, the $\chi_M T$ for **1** remains constant until ∼70 K and then shows an abrupt decrease to reach a value of 5.44 $cm^3$ $mol^{-1}$ K at 2 K. This behavior is due to a combination of intramolecular antiferromagnetic interactions between $Mn^{III}$ and $Gd^{III}$ ions and zero-field splitting effects mainly of the $Mn^{III}$ ion and to lesser extent of the $Gd^{III}$ ion (the temperature dependence of $\chi_M T$ cannot be reproduced taking into account only the zfs of the $Mn^{III}$ ion).

The magnetic properties of these compounds have been modeled by using the following Hamiltonian:

$$\hat{H} = -J\hat{S}_{Mn}\hat{S}_{Gd} + D_{Mn}\hat{S}^2_{MnZ} + g\mu_B\hat{S}_{Mn}H + g\mu_B\hat{S}_{Gd}H$$

where $J$ accounts for the magnetic exchange coupling between $Gd^{III}$ and $Mn^{III}$ ions, $D_{Mn}$ accounts for the axial single-ion zero-field splitting parameter of the $Mn^{III}$ ion ($D_{Gd}$ is assumed to be negligible as this ion is rather isotropic), and the two last terms represent the corresponding Zeeman effects. As $J$ and $D_{Mn}$ are strongly correlated and provoke the same result at low temperature, these parameters cannot be accurately determined from the fit of the susceptibility and magnetization data. In view of this and to extract an accurate $J$ value, we decided to determine the $D_{Mn}$ value from precise *ab initio* calculations (see below) and then the calculated value ($D_{Mn} = -3.08$ $cm^{-1}$) fixed in the above Hamiltonian. The simultaneous fit of the experimental susceptibility and magnetization data with this Hamiltonian using the full-matrix diagonalization PHI program[15] afforded the following set of parameters: $J = -0.5$ $cm^{-1}$ and $g = 2.06$ $cm^{-1}$ {$R = 1.8 \times 10^{-4}$ ($R = \sum[(\chi_M T)_{exp} - (\chi_M T)_{calcd}]^2/\sum(\chi_M T)_{exp})^2$}. The extracted $J$ value is almost


DOI: 10.1021/acs.inorgchem.7b02917
Inorg. Chem. 2018, 57, 3683−3698

Table 1. Selected Bond Distances (Å) and Angles (deg) of 1−4[a]

| | | | 1 | 2 | 3 | 4 |
|---|---|---|---|---|---|---|
| Mn1 | Ln1 | | 3.4591(8) | 3.4391(6) | 3.428(1) | 3.4238(9) |
| Mn1 | O1 | | 1.833(3) | 1.836(2) | 1.849(4) | 1.841(4) |
| Mn1 | O2 | | 1.925(3) | 1.926(2) | 1.920(5) | 1.924(4) |
| Mn1 | O5 | | 1.924(5) | 1.918(4) | 1.913(7) | 1.917(6) |
| Mn1 | O8 | | 2.293(3) | 2.301(2) | 2.294(5) | 2.294(4) |
| Mn1 | N8 | | 2.089(5) | 2.095(4) | 2.096(6) | 2.090(5) |
| Mn1 | N18 | | 2.436(4) | 2.438(3) | 2.433(5) | 2.434(5) |
| Ln1 | O2 | | 2.374(4) | 2.340(3) | 2.337(6) | 2.318(5) |
| Ln1 | O4 | | 2.627(5) | 2.621(3) | 2.610(7) | 2.610(6) |
| Ln1 | O5 | | 2.348(5) | 2.325(3) | 2.316(6) | 2.311(5) |
| Ln1 | O6 | | 2.395(5) | 2.370(3) | 2.348(8) | 2.343(5) |
| Ln1 | O7 | | 2.376(4) | 2.345(3) | 2.332(6) | 2.316(5) |
| Ln1 | O11 | | 2.498(6) | 2.458(3) | 2.453(7) | 2.453(6) |
| Ln1 | O12 | | 2.507(5) | 2.480(4) | 2.456(6) | 2.460(5) |
| Ln1 | O14 | | 2.458(4) | 2.418(3) | 2.418(5) | 2.407(4) |
| Ln1 | O15 | | 2.456(3) | 2.445(3) | 2.439(5) | 2.414(5) |
| Mn1 | O2 | Ln1 | 106.7(2) | 107.0(1) | 107.0(1) | 107.2(2) |
| Mn1 | O5 | Ln1 | 107.7(2) | 107.9(1) | 107.9(1) | 107.8(3) |

[a]Gd (**1**), Dy (**2**), Ho (**3**), Er (**4**).

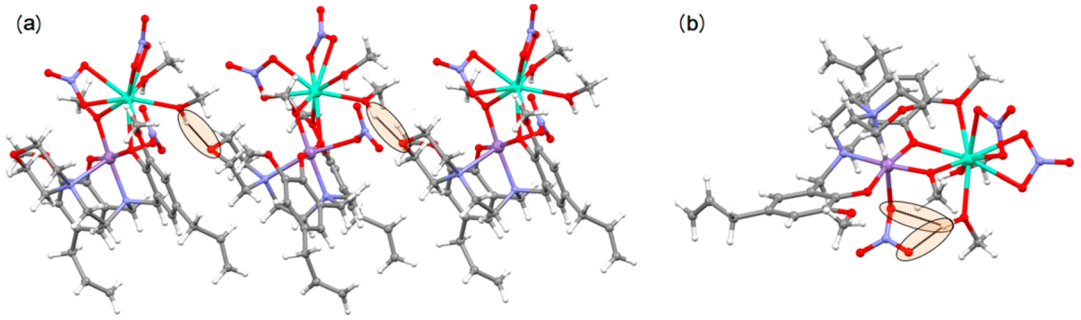


**Figure 3.** (a) Inter- and (b) intramolecular hydrogen bonding in complex **1**.

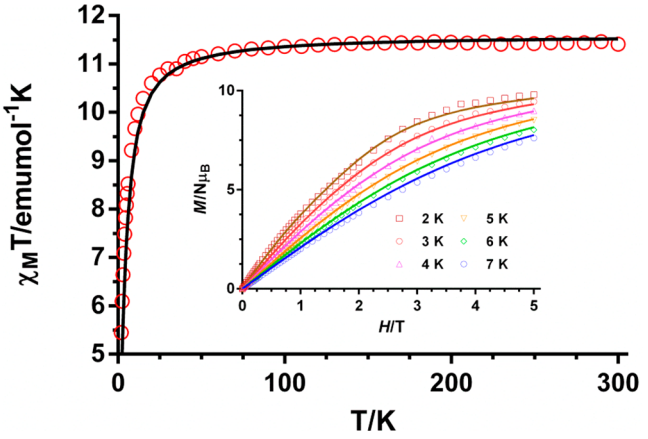


**Figure 4.** Temperature dependence of the $\chi_M T$ for **1**. Inset: Field dependence and temperature dependence of the magnetization. Solid lines represent the best fit of the experimental data with the parameters indicated in the main text.

insensitive to changes in $D_{Mn}$ between −2 and −4 $cm^{-1}$, which points out its consistency. Moreover, this value is similar to that found for an alkoxo/hydroxo bridged tetranuclear complex $Mn^{III}_2Gd^{III}_2$ of −0.32 $cm^{-1}$.[13j]

The field dependence of the magnetization at 2 K for **1** (inset of Figure 1) shows a slow increase of the magnetization at low field, in accord with the antiferromagnetic interaction between $Mn^{III}$ and $Gd^{III}$, and a quasilinear increase at high field without achieving complete saturation even at 5 T. This behavior suggests the presence of significant magnetic anisotropy and/or the existence of low-lying excited states that are partially populated at this temperature. The low-lying excited states are in agreement with the weak magnetic interactions expected for $Mn^{III}Gd^{III}$ systems. The magnetization value for **1** at 5 T of $9.80N\mu_B$ is lower than the expected saturation magnetization value, $M_s/N\mu_B = 11.38N\mu_B$ with $g = 2.07$, which is due to the presence of antiferromagnetic interactions between the metal ions as well as to the local magnetic anisotropy of the $Mn^{III}$ ion.

**Magneto-thermal Properties of 1.** The magneto-thermal properties of **1** have been analyzed because (i) the antiferromagnetic interactions between the $Gd^{III}$ and $Mn^{III}$ ions are very weak and therefore make this system appropriate for large MCE, (ii) the $Gd^{III}$ ion shows negligible anisotropy due to the absence of orbital contribution, (iii) the $Gd^{III}$ exhibits the large single-ion spin ($S = 7/2$) arising from the $4f^7$ electron configuration, and finally (iv) although the $Mn^{III}$ ion possesses magnetic anisotropy due to Jahn−Teller distortion, it exhibits a comparatively high spin ($S = 2$) and a large maximum entropy value (calculated as $R\ln(2S_{Mn} + 1)/M_{Mn} = 271$ J $kg^{-1}$ $K^{-1}$). In view of the above considerations, compound **1** could be a good candidate for magnetic coolers.

The magnetic entropy changes ($-\Delta S_m$) that determine the magnetocaloric properties of **1** can be extracted from the


DOI: 10.1021/acs.inorgchem.7b02917
Inorg. Chem. 2018, 57, 3683−3698

experimental isothermal field-dependent magnetization data (Figure 5) using the Maxwell relation:

$$\Delta S_M = (T, \Delta B) = \int_{B_i}^{B_f} \left[\frac{\partial M(T, B)}{dT}\right]_B dB$$

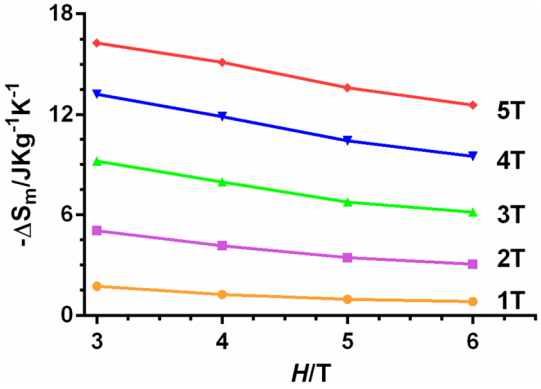


**Figure 5.** Magnetic entropy changes extracted from the experimental magnetization data with the Maxwell equation from 1 to 5 T and temperatures from 3 to 6 K (points). Solid lines are a guide for the eye.

where $B_i$ and $B_f$ are the initial and final applied magnetic fields. The values of $-\Delta S_M$ for **1** under all fields increase as the temperature decreases from 6 to 3 K. This compound attains a maximum value of $-\Delta S_m$ = 16.82 J kg$^{-1}$ K$^{-1}$, $T$ = 3 K and applied field change $\Delta B$ = 5 T (Figure 5). Despite the antiferromagnetic interaction between the Gd$^{III}$ and Mn$^{III}$ ions, a considerable change in $-\Delta S_m$ occurs, which is compatible with easy spin polarization at relatively low magnetic field. It is worth mentioning that, due to limitations of our instrument, the $-\Delta S_m$ at about 2 K could not be obtained, but it is expected to be larger than 16.82 J kg$^{-1}$ K$^{-1}$ as $-\Delta S_m$ increases when lowering the temperature. The extracted $-\Delta S_m$ values at $T$ = 3 K and at 5 T for **1** are much smaller than that calculated for the full magnetic entropy content per mole $R$ ln($2S_{Gd}$ + 1) + $R$ ln($2S_{Mn}$ + 1) = 3.69, $R$ = 31.60 J kg$^{-1}$ K$^{-1}$, which is likely due to the antiferromagnetic interaction between Mn$^{III}$ and Gd$^{III}$ and the magnetic anisotropy of the Mn$^{III}$, as the increase of these two factors is known to diminish the MCE. Nevertheless, the extracted $-\Delta S_m$ value at 5 T and 3 K is similar to those found for Gd$^{III}_4$Mn$_4^{II}$ complexes[16] but larger than those observed for Gd$^{III}_6$Mn$_{12}^{II}$ complexes[17] with a Gd/Mn = 0.5. The MCE increases with the increase of the Gd/Mn ratio as expected for increasing the spin and diminishing the magnetic anisotropy.

**Theoretical Calculations on complex 1.** *Magnetic Anisotropy of the Mn$^{III}$ Center.* In order to support the $D_{Mn}$ value extracted from magnetic measurements for compound **1**, we have performed post-Hartree−Fock *ab initio* calculations using the MOLCAS8.0 package.[18,19] For estimation of the zero-field parameter of Mn$^{III}$, Gd$^{III}$ was replaced by Lu(III). Calculations afford $D_{Mn}$ = −3.08 cm$^{-1}$ with $E/D$ = 0.11 cm$^{-1}$. The $D_{Mn}$ values agree with the expected single-ion values reported in the literature.[20] The orientation of the **D**-tensor is shown in Figure 6 and the $D_{zz}$ axis nearly coincides with the Jahn−Teller (JT) elongated axis.

**Estimation of Exchange coupling Constant in 1 Using DFT.** While ferromagnetic coupling for different {3dGd} complexes is common, there are only a few examples where antiferromagnetic coupling for {3dGd} has been observed.[10c,12a,c,21] Although extensive assessment methods have been undertaken by us[12a] and others for the {CuGd} pair,[12f,g] a rigorous benchmarking, which include antiferromagnetic exchange, has not been studied in detail. Here, we intend to address this issue.

**Assessing Suitable Methodology for *J* Calculation in 1.** To assess a suitable methodology for computing $J$ values for **1**, we have chosen various hybrid and nonhybrid exchange-correlation functionals with a variety of local and exchange correlation to understand how the magnetic coupling is influenced by the nature of the functional. The test includes several GGA, meta-GGA functionals with varying percentages of HF exchange. Additionally, we have also tested both all-electron and effective core potential basis set effects on the nature of magnetic coupling. Basis set effects are studied using the B3LYP functional in combination with the ECP basis set such as CSDZ[22] and CRENBL[23] along with the Nakajima all-electron basis set[24] incorporating relativistic effect using DKH methodology[25] for the Gd(III) ion (Table 2). For other atoms,

**Table 2. DFT Computed *J* Values with B3LYP Functional and Different Basis Sets**

| basis set | $J$/cm$^{-1}$ | $\langle S^2\rangle$ (HS, BS) | description | relativistic |
|---|---|---|---|---|
| CSDZ | 0.01 | 35.801, 7.729 | Gd(CSDZ ECP), TZV for others | ECP |
| CSDZ | 0.04 | 35.802, 7.803 | Gd(CSDZ ECP), TZVP for others | ECP |
| Nakajima | −1.13 | 35.789, 7.788 | Gd(Nakajima all e$^-$), TZV for others | DKH |
| Nakajima | −1.15 | 35.790, 7.789 | Gd(Nakajima all e$^-$), TZVP for others | DKH |
| CRENBL | −0.11 | 35.791, 7.791 | Gd(CRENBL ECP), TZV for others | ECP |
| CRENBL | −0.12 | 35.792, 7.792 | Gd(CRENBL ECP), TZVP for others | ECP |

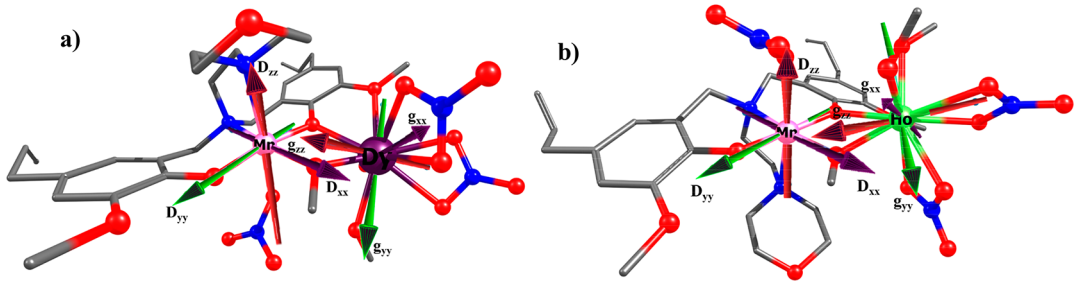


**Figure 6.** (a) Orientation of the **g**-tensors of Dy$^{III}$ and **D**-tensors of the Mn$^{III}$ ion in complex **2**. (b) Orientation of the **g**-tensors of Ho$^{III}$ and **D**-tensors of the Mn$^{III}$ ion in complex **3**.



DOI: 10.1021/acs.inorgchem.7b02917
*Inorg. Chem.* 2018, 57, 3683−3698

Ahlrichs TZV or TZVP was used.[26] Two combinations of basis sets employed with CSDZ predict, contrary to the experimental estimate, weak ferromagnetic coupling between $Mn^{III}$ and $Gd^{III}$ ions (see Table 2). While the B3LYP/CSDZ combination was found to yield a good numerical estimate for several {3dGd} pairs earlier, here this combination was found to overestimate the ferromagnetic contribution to the net exchange. This may be correlated to the fact that the net antiferromagnetic coupling constant $J$ observed is very small and the estimated $J$ values are sensitive to the basis set employed. While the Nakajima basis set incorporating the DKH relativistic effect reproduces the sign correctly, the magnitudes of the $J$ values are overestimated compared to the experimental value. The CRENBL basis set was found to yield $J$ values which are of the correct sign and are closer to the experimental estimate, and we have therefore employed this basis set to assess various exchange-correlation functionals.

Computed $J$ values with different functionals in combination with CRENBL ECP are given in Table 3. Two pure functionals

**Table 3. DFT Computed $J$ Values with Different Functionals Using CRENBL ECP Basis Set**

| functional | $J$/cm$^{-1}$ | $\langle S^2 \rangle$ (HS, BS) | spin density on (Gd, Mn) at HS state | % of HF exchange |
|---|---|---|---|---|
| exptl | −0.50 | | | |
| BLYP | 0.55 | 35.787, 7.787 | 7.080, 3.674 | 0% |
| BP86 | 1.69 | 35.804, 7.801 | 7.186, 3.711 | 0% |
| B3LYP | −0.11 | 35.791, 7.791 | 7.057, 3.834 | 20% |
| X3LYP | −0.18 | 35.791, 7.791 | 7.051, 3.843 | 21.8% |
| B98 | −0.83 | 35.797, 7.797 | 7.069, 3.864 | 21.98% |
| SB98 | −0.83 | 35.797, 7.797 | 7.069, 3.864 | 21.98% |
| mPW1PW91 | 0.03 | 35.809, 7.809 | 7.138, 3.917 | 25% |
| BH and H | −0.45 | 35.791, 7.791 | 7.020, 3.930 | 50% |
| BH and HLYP | −0.30 | 35.787, 7.787 | 7.001, 3.937 | 50% |

tested (BLYP and BP86) yield the wrong sign, while inclusion of HF exchange improves the estimates and in fact yields the correct sign in most of the functionals tested. While increasing the percentage of HF exchange tends to improve the estimated $J$ values, all hybrid functionals (with the exception of mPW1PW91) yield weak antiferromagnetic coupling. For developing mechanism and magneto-structural correlations, we have employed the B3LYP functional as this has been the work-horse functional for the estimation of magnetic coupling in several examples reported earlier.[27]

**Mechanism of Magnetic Coupling in {$Mn^{III}Gd^{III}$} Pair.** When a suitable method was assessed, we moved forward trying to understand the mechanism of magnetic coupling in the {$Mn^{III}Gd^{III}$} pair. A general schematic mechanism adapted from earlier {CuGd} complexes is shown in Figure 7. The net exchange coupling between the $Mn^{III}$ and $Gd^{III}$ ions has two contributions: (i) The first is the antiferromagnetic contribution that solely arises from the overlap between the single occupied magnetic orbitals (SOMOs) of the $Mn^{III}$ ions with the 4f orbitals of the $Gd^{III}$ ion (see Figure S1 in Supporting Information). However, this overlap is expected to be weak as the 4f orbitals are inert in nature and do not mix strongly with the ligand orbitals, and (ii) the second factor is the ferromagnetic contribution to the exchange that arises from orbital orthogonality between the SOMOs of 3d and $Gd^{III}$ ion, as well from a charge-transfer process from the $Mn^{III}$ to the formally empty 5d orbitals of $Gd^{III}$. This charge-transfer

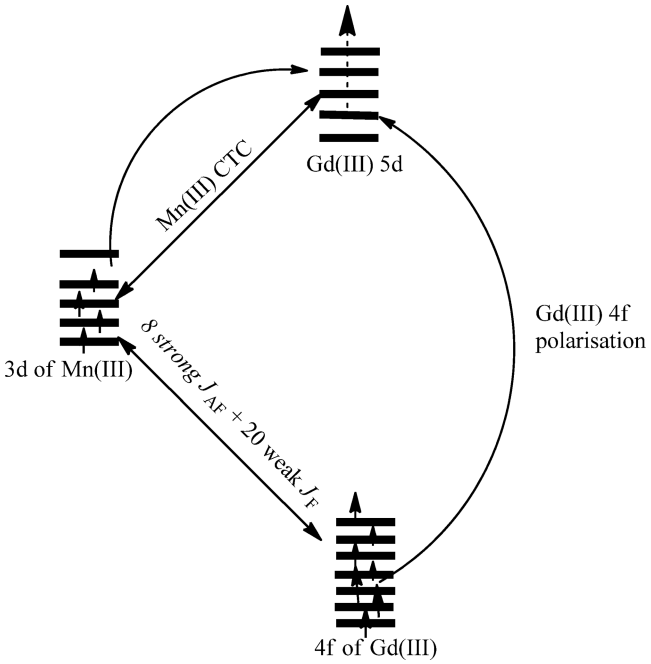


**Figure 7.** Schematic mechanism for the magnetic coupling for the {$Mn^{III}Gd^{III}$} pair obtained from the DFT calculations. The nature and the number of interactions between the $Mn^{III}$ and the $Gd^{III}$ are shown by double headed arrows. The $Gd^{III}$ 5d orbitals gain density via the $Mn^{III}$ charge-transfer and via 4f polarization.

contribution will ensure the same spin orientation for the 4f orbitals leading to a ferromagnetic coupling.

The magnetic coupling in complex **1** has four superexchange pathways: the first two are through the OMe and OPh bridges, and the third and fourth are through H-bonding between the coordinated methanol and the nitrate group and the long alkyl linker connecting the two metal ions, respectively. Overlap integrals computed between the SOMOs of the $Mn^{III}$ ion and 4f orbitals of $Gd^{III}$ reveal a significant overlap for several pairs. Particularly, both the $d_{xz}$ and $d_{yz}$ orbitals of the $Mn^{III}$ ions were found to overlap with several 4f orbitals as shown in Figure 8 (see Tables S1 and S2 in Supporting Information). Among the 28 possible overlaps, eight overlaps are very significant, rendering a large contribution to the antiferromagnetic part of the exchange. This is rather unusual, as generally the overlaps between the 3d and 4f orbitals are weak. However, in this case, after a close examination of all the 4f orbitals, it has become clear that $\sigma^*$-antibonding orbitals of the OMe group are strongly overlapping with some of the 4f orbitals (see Figure S1 in Supporting Information), and this promotes strong overlap leading to a net antiferromagnetic exchange. To probe this effect further, we have performed additional calculations on model systems (model 1a, see Figure S2 in Supporting Information) where fictitiously the OMe group is removed and replaced by a computed point-charge to avoid alterations to the crystal field effect of the metal ions. These calculations yield a ferromagnetic coupling ($J$ = 1.6 cm$^{-1}$), clearly suggesting that the OMe group promotes antiferromagnetic exchange (Table S3 in Supporting Information). This is also supported by our QTAIM analysis (see below). Additionally, the overlap integral calculations performed on this model suggest a significant drop in the computed 3d/4f overlap values compared to those of complex **1** (see Table S4 in Supporting Information). To probe if the effect is due to the presence of the $Mn^{III}$ ion, an additional


DOI: 10.1021/acs.inorgchem.7b02917
Inorg. Chem. 2018, 57, 3683−3698

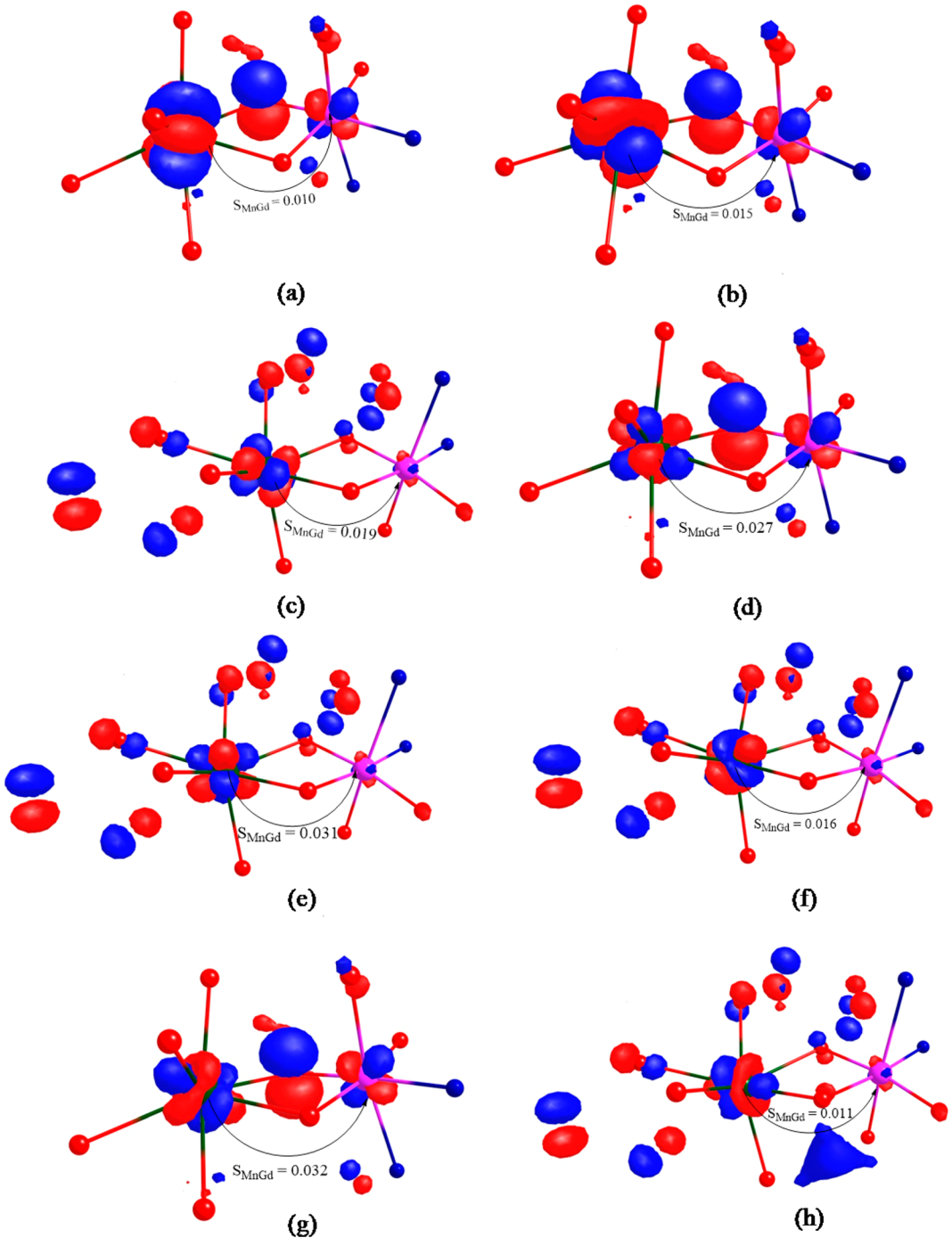


**Figure 8.** (a–h) Overlap of 4f orbitals of $Gd^{III}$ with the $3d_{xz}/3d_{yz}$ orbitals of $Mn^{III}$. For clarity, only the core structure is shown with orbital lobes, and the other atoms are not shown.

factious model (model 1b) is constructed where the $Mn^{III}$ ion is replaced by the $Gd^{III}$ ion and this renders ferromagnetic coupling, supporting the mechanistic aspects proposed above.

We have then examined the ferromagnetic contribution to the net exchange. The $Mn^{III}$ ion possesses unpaired electrons in $d_{xy}$, $d_{xz}$, $d_{yz}$, and $d_{z^2}$ orbitals due to the Jahn–Teller elongation. The computed spin density plot with the B3LYP/CRENBL setup is shown in Figure 9 (Figure S3 and Table S5). The $Gd^{III}$ ion is propagating the spin polarization as is evident from negative spin densities on the atoms coordinated to the $Gd^{III}$ ion while the $Mn^{III}$ propagates a mixture of spin delocalization and polarization. The spin delocalization is particularly visible on the ligand that lies along the $d_{z^2}$ orbital direction (see Figure 9). The main contributions to the Mn(3d) → Gd(5d) charge-

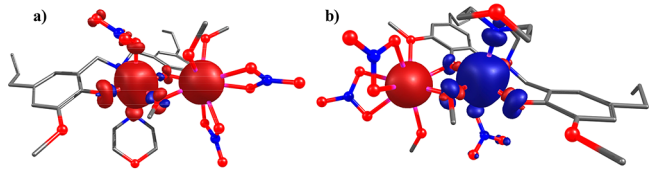


**Figure 9.** Computed spin density of the (a) high-spin and (b) broken-symmetry state of complex **1**.



DOI: 10.1021/acs.inorgchem.7b02917
*Inorg. Chem.* 2018, 57, 3683–3698

transfer generally arise from a $\sigma$-type $d_{z^2}$ orbital; however, here the $d_{z^2}$ orbital is perpendicular to the bridging OMe and OPh groups rendering only a weak charge-transfer via an H-bonding pathway. The NBO analysis indicates that both 6s and 5d orbitals have significant populations (Table S6 in Supporting Information) and, particularly, 5d orbitals have the partial occupation of 0.47e. This is marginally lower compared to the {CuGd} pair studied revealing less of a ferromagnetic contribution, leading to an overall antiferromagnetic coupling in complex **1**.

To gain further understanding on the bonding and nature of the charge-transfer, the quantum theory of atoms in molecules (QTAIM) was applied to depict the topological properties of complex **1**. To better understand the nature of the interaction of the Ln atom with others, we have used Bader's atoms in molecules theory.[28] Bader and co-workers characterize bonding and nonbonding interactions of atoms in terms of topological properties such as electron density $\rho(r)$, Laplacian of the electron density $L(r)$, potential energy density $V(r)$, kinetic energy density $G(r)$, total energy density $H(r)$, and potential energy to the Lagrangian kinetic energy ratio $|V(r)|/G(r)$. For instance, the presence of a (3, −1) critical point in QTAIM topography represents a chemical bond between two atoms, and these are called the bond critical points (BCPs), where the shared electron density reaches a minimum, whereas a critical point with (3, +1) and (3, +3) signatures identifies a ring structure (RCP) and cage critical point (CCP) in the molecular system, respectively. The $\rho(r)$ values at the BCPs are related to the strength of the bonds.[29]

We have investigated the topological properties at the bond critical point (BCPs) for complex **1** and other model complexes. QTAIM analysis clearly displays BCPs indicating the bonded and the nonbonded interactions that exist in the complexes. In the molecular graph (Figure 10), the big circles

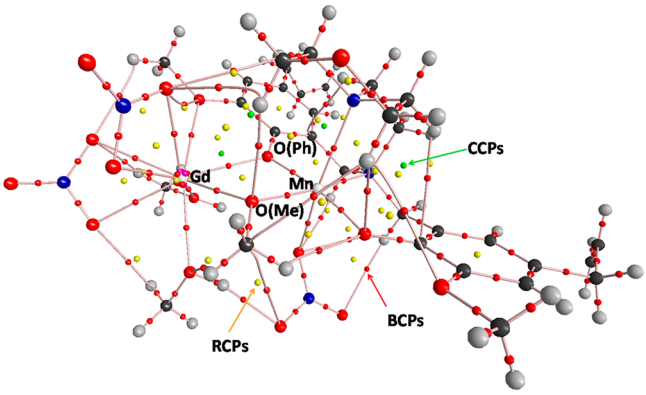


**Figure 10.** Molecular graph of **1**. Solid lines indicate bond paths, and large circles correspond to attractors, small red ones to BCPs, yellow ones to RCPs, and green ones to CCPs.

correspond to attractors attributed to positions of atoms and critical points such as (3, −1) BCP (red), (3, +1) RCP (yellow), and (3, +3) CCP (green) indicated by small circles. The topological properties at BCPs for $Mn^{III}$ and $Gd^{III}$ coordinated atoms are collected in Tables S7 and S9 in Supporting Information. The $Gd^{III}$ atom forms bonds with the nine O atoms of the coordinated ligands which is indicated by nine BCPs whereas the $Mn^{III}$ atom forms six bonds with four O atoms and two N atoms of the coordinated ligand, confirmed by six BCPs (see Figure 10). The electron density $\rho(r)$ at the BCP between Gd/Mn and the O atoms is small (Gd−O = 0.0273 au < $\rho(r)$ < 0.0432 au and Mn−O = 0.1395 au < $\rho(r)$ < 0.0776 au), and $\nabla^2_{\rho(r)}$ is small and positive (Gd−O = 0.0198 au < $\nabla^2_{\rho(r)}$ < 0.0530 au and Mn−O = 0.2054 au < $\nabla^2_{\rho(r)}$< 0.0711 au), indicating a closed-shell character of the coordination bonds.[30] The partly covalent nature of the investigated interactions can be supported by the $|V(r)|/G(r)$ ratio;[30,31] $|V(r)|/G(r)$ < 1 is characteristic of a typical ionic interaction, and $|V(r)|/G(r)$ > 2 is diagnostic of a "classical" covalent interaction. The QTAIM-defined topological properties at Gd−OPh, Gd−OMe, Mn−OPh, and Mn−OMe BCPs indicate a mixed (largely ionic with significant covalent component) character of these coordination bonds, and this is also supported by the $|V(r)|/G(r)$ < ∼1.1 found for complex **1**. In a comparison with Mn−O(Me) and Mn−O(Ph) bonds, the Mn−O(Me) bonds possess higher $H(r)$ values, and hence, the Mn−O(Me) bonds have a more covalent nature than the Mn−O(Ph) bonds. The Mn−O(Me) bond is stronger compared to the Mn−O(Ph) bond as revealed by the higher $\rho(r)$ values for the former. The same is observed also for Gd−O bonds. The Laplacian function $\nabla^2_{\rho(r)}$ at the BCP between $Mn^{III}$ and the equatorial ligand atoms shows higher values in the 0.07−0.16 au range, whereas the axial ligand shows small $\nabla^2_{\rho(r)}$ values between 0.03 and 0.04 au. This suggests that the axial ligands are weaker as could be expected from the JT elongated structures.

**Magneto-Structural Correlations in $Mn^{III}$–$Gd^{III}$ Complexes.** Magneto-structural correlations are very useful tools to interpret the observed magnetic properties of novel complexes in order to design new compounds with improved magnetic properties. Different magneto-structural correlations have been found on $Mn^{III}$–$Gd^{III}$ complexes by varying Mn−O−Gd angles (keeping the dihedral fixed at ∼12°) and Mn−O−Gd−O dihedrals. The average bond angle versus $J$ plot is shown in Figure 11.

As can be observed from the above figures, $J$ values increase linearly with the Mn−O−Gd bond angle and become ferromagnetic for angle values higher than ∼107°. At a lower angle, the structure is more compact, and the overlap between the magnetic orbital increases, leading to an antiferromagnetic coupling, while at higher angles the overlap between the SOMOs of $Mn^{III}$ and $Gd^{III}$ diminishes, leading to a ferromagnetic coupling (see Table S1 in Supporting Information). Moreover, at large Mn−O−Gd angles, the charge-transfer contribution also enhances, leading to a steady increase in the ferromagnetic coupling. The spin densities of the $Mn^{III}$ center are found to gradually decrease with the increasing Mn−O−Gd angle, and at the same time, the spin density of the $Gd^{III}$ is also found to increase. This suggests that $Mn^{III}$ promotes stronger delocalization (polarization) at higher angles, and this is correlated to the magnitude of the computed exchange coupling constant (see Figure 11, right).

The correlation developed by varying the Mn−O−Gd−O dihedral angle (keeping the average Mn−O−Gd angle fixed ∼107°) is shown in Figure 12. As the Mn−O−Gd−O dihedral angle increases, the ferromagnetic contribution to the net exchange decreases, and this continues until the angle reaches ∼11.15°. Afterward, the contribution increases leading to a net ferromagnetic coupling. Therefore, ferromagnetic interactions are observed at both low and high dihedral angles. This is well-supported by our QTAIM analysis (see below). Complex **1** has a Mn−O−Gd−O dihedral of 11.2°, and decreasing this angle leads to a weakening of the 3d/4f overlap with a concomitant


DOI: 10.1021/acs.inorgchem.7b02917
Inorg. Chem. 2018, 57, 3683−3698

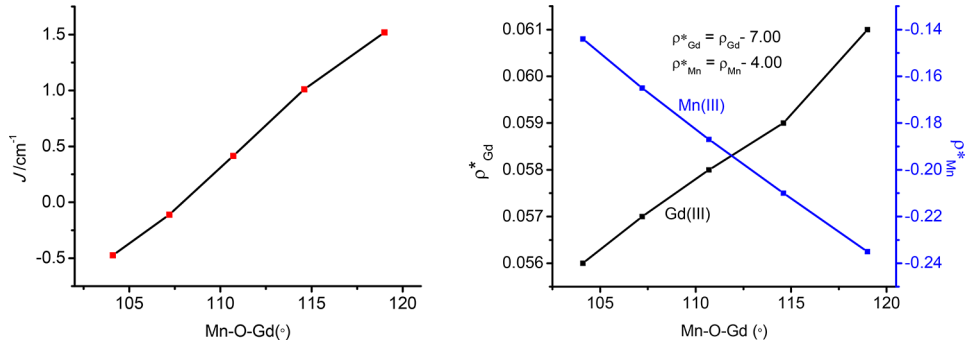


**Figure 11.** Magneto-structural correlations developed by varying the average Mn−O−Gd angle plotted against corresponding $J$ values (left). Computed spin densities at the $Mn^{III}$ and $Gd^{III}$ ions for various Mn−O−Gd angles at the same point (right).

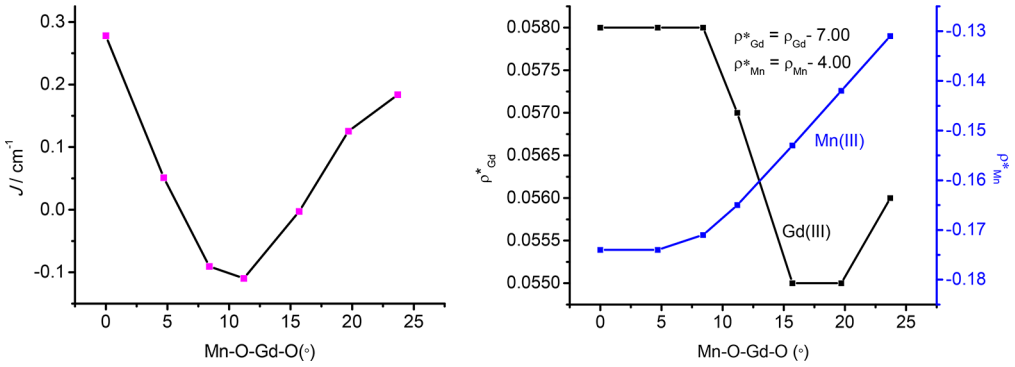


**Figure 12.** Magneto-structural correlations developed by varying Mn−O−Gd−O dihedral (left) plotted against corresponding $J$ values and the computed $Mn^{III}$ and $Gd^{III}$ spin densities at the same point (right).

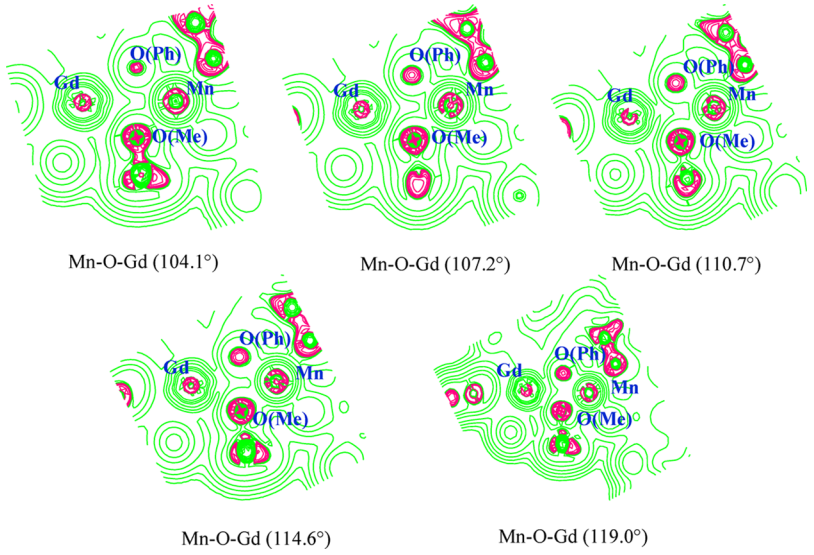


**Figure 13.** Contour line diagram of the Laplacian of electron density along the Mn−O−Gd−O plane. Solid green lines indicate charge depletion $[\nabla^2_{\rho(r)} > 0]$, and solid red lines indicate charge concentration $[\nabla^2_{\rho(r)} < 0]$.

increase of the ferromagnetic contribution by charge-transfer, leading to a net ferromagnetic coupling at lower dihedral angles. This trend is similar to that observed in the {CuGd} pair. At higher dihedral angles beyond 10.5°, a similar trend is again visible where the prominent Mn($d_{xz}$/$d_{yz}$)−Gd(4f) orbital overlap diminishes, leading to a drastic reduction in the $J_{AF}$ contribution and hence to a net ferromagnetic coupling (see Table S1 in Supporting Information). A similar variation in the $Mn^{III}$ and $Gd^{III}$ spin densities is visible also for this parameter (see Figure 12, right)

To investigate the developed correlations further, we have performed QTAIM analysis for the correlation points. Calculations reveal that both the $\rho(r)$ and $\nabla^2_{\rho(r)}$ values increase linearly with the Mn−O−Gd bond angle (see Figures S5 and S6 in Supporting Information). However, the $H(r)$ values decrease linearly with the increase in the Mn−O−Gd angle, and this suggests that a larger Mn−O−Gd angle enhances the covalency of the metal−ligand bonds. These results are in line with the $|V(r)|/G(r)|$ ratio and our magneto-structural findings. The Mn−O(Me) and Gd−O(Me) bonds are found to be more


DOI: 10.1021/acs.inorgchem.7b02917
Inorg. Chem. 2018, 57, 3683−3698

covalent in nature with higher $H(r)$ values compared to other bonds. This supports the assessment that the OMe group promotes antiferromagnetic exchange (see also Table S3 in Supporting Information).

The correlation proposed between Mn−O(Me) and Mn−O(Ph) QTAIM parameters and the Mn−O−Gd−O dihedral angle is shown in Figures S6 and S7. As the Mn−O−Gd−O dihedral increases, the $\rho(r)$ and $\nabla^2_{\rho(r)}$ values decrease slowly. Figure 13 shows the contour plot Laplacian function $\nabla^2_{\rho(r)}$ through the Mn−O−Gd−O plane. The valence shell charge concentration (VSCC) zone of the bridging O atom is diffused toward the $Gd^{III}$ and $Mn^{III}$ atoms. This indicates that there is a charge-transfer from the bridging O atom. However, the VSCC zone of the O(Me) group is more diffused toward the C atom of the methyl group, and the VSCC zone decreases with increasing Mn−O−Gd angle. Hence, the QTAIM analysis clearly highlights the importance of the bridging OMe group.

**Magnetic Properties of Compounds 2−4.** We now discuss the magnetic properties of compounds **2**, **3**, and **4**, which are shown in Figure 14. At room temperature, the $\chi_M T$

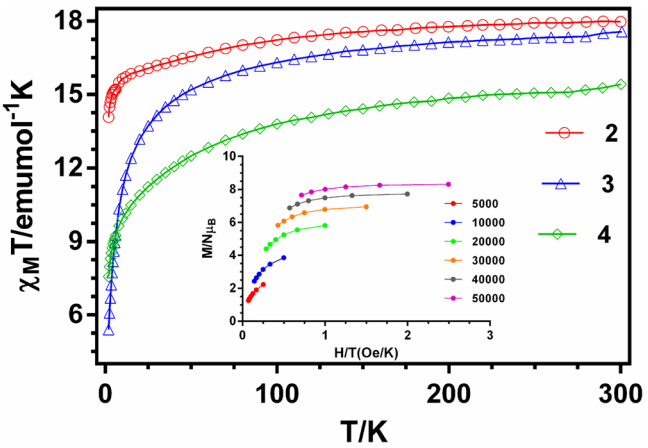


**Figure 14.** Temperature dependence of the $\chi_M T$ for **2**−**4**. Inset: Magnetization vs $H/T$ plot for compound **2**.

values for these complexes (17.98, 17.56, and 15.41 $cm^3$ K $mol^{-1}$, respectively) are slightly higher than those calculated (17.17, 17.07, and 14.48, respectively) for one $Mn^{III}$ ($S = 2$ with $g_{Mn} = 2.0$) and one $Ln^{III}$ ($Dy^{III}$ $4f^9$, $J = 15/2$, $S = 5/2$, $L = 5$, $^6H_{15/2}$, $g_J = 4/3$; $Ho^{III}$, $L = 6$, $S = 2$, $J = 8$, $g_J = 5/4$, $5I_8$; $Er^{III}$, $L = 6$, $S = 3/2$, $J = 15/2$, $g_J = 6/4$, $^4I_{15/2}$) noninteracting ions in the free-ion approximation.

$$\chi_M T = \frac{N\beta^2}{3k}\{g_j^2 J(J+1) + g_{Mn}^2 S(S+1)\}$$

On lowering the temperature, the $\chi_M T$ decreases with decreasing temperature, first slowly down to ∼60 K and then rapidly exhibiting a very sharp decrease below ∼12 K (to reach values of 14.1, 5.4, and 7.6 $cm^3$ $mol^{-1}$ K at 2.0 K for **2**−**4**, respectively). The decrease observed in $\chi_M T$ is most likely due to a combination of the thermal depopulation of the $M_J$ sublevels of the $^{2S+1}\Gamma_J$ ground state of the $Ln^{3+}$ ion, which is split by ligand field effects, and some very weak $Mn^{3+}\cdots Ln^{3+}$ antiferromagnetic interactions. The existence of very weak antiferromagnetic interactions in complexes **2**−**4** is not unexpected because isostructural $Gd^{3+}$, $Tb^{3+}$, $Dy^{3+}$, and $Ho^{3+}$ complexes generally display magnetic exchange interactions of the same nature.

The field dependence of the magnetization at 2 K for compounds **2**−**4** (Figure S8) reveals a relatively slow increase of the magnetization at low fields and then a linear increase without clear saturation above 1 T. The linear high-field variation of the magnetization suggests the presence of a significant magnetic anisotropy and/or low-lying excited states that are partially populated at this temperature. The presence of low-lying excited states close in energy to the ground state is compatible with the weak magnetic exchange interactions between $Mn^{III}$ and $Ln^{III}$ ions expected for these compounds. It should be noted that the magnetization values at the highest applied dc magnetic field of 5 T are, however, almost half of those calculated for noninteracting $Mn^{III}$ and $Ln^{III}$ ions (Table 2), which is, as usual, mainly attributed to crystal field effects giving rise to significant magnetic anisotropy. $M$ versus $H/T$ data (Figure 13 inset, the plot for compound **2** is given as an example) are not superimposed on a master curve, thus supporting the presence of a significant anisotropy and/or low-lying excited states.

Dynamic ac magnetic susceptibility measurements as a function of temperature at different frequencies and under zero external field show that only complex **2** exhibits slight frequency dependence in the out-of-phase ($\chi''_M$) signals below ∼4.5 K, but without reaching a maximum, probably because either the thermal energy barrier for the reorientation of the magnetization is very low or there exists overlapping with a faster quantum tunnelling relaxation process, even at frequencies as high as 1400 Hz. However, the $\chi''_M$ signal is quite weak with a $\chi''_M/\chi'_M$ ratio of ∼0.01. When the ac measurements were performed in the presence of a small external dc field of 1000 G to suppress fully or partly the quantum tunnelling relaxation of the magnetization (QTM), the intensity of the signals from compounds **2** and **4** drastically increases but again without showing a maximum above 2 K (Figure S9). These results indicate that, despite the magnetic anisotropy of both the $Mn^{III}$ and $Ln^{III}$ ions, the thermal energy barrier is too small to observe a maximum in the $\chi''_M$ versus $T$ plot above 2 K, and thus, clear SMM behavior is not observed. This is likely due the nonfavorable orientation of the main local anisotropies axes of $Mn^{III}$ and $Ln^{III}$ ions leading to a relatively weak anisotropy for the whole molecule and to the existence of weak antiferromagnetically coupling between $Mn^{III}$ and $Ln^{III}$ ions, which allows mixing of the low-lying excited states in the ground state, thus favoring fast QTM and quenching the slow relaxation of the magnetization. Moreover, the distribution of oxygen atoms around the $Ln^{III}$ ions is not appropriate to afford either a strong axial crystal field or an easy-plane crystal field, which would favor SMM behavior in **2** and **4**, respectively.

**Theoretical Calculations on Complexes 2 and 3.** To understand the slow relaxation of magnetization in {$Mn^{III}Dy^{III}$} complex **2** and to probe the nature and magnitude of the exchange interactions, we have performed CASSCF *ab initio* calculations on the mononuclear fragments such as {$Mn^{III}La^{III}$} and {$Co^{III}Dy^{III}$} models and utilized the computed data to fit the susceptibility using the Lines approach employing the POLY_ANISO module.[32]

The mechanism of magnetization relaxation developed for the single-ion $Dy^{III}$ is shown in Figure 15a. The energy span of eight Kramers doublets (KDs) is found to lie within an energy window of 374.2 $cm^{-1}$ with the ground state of the $Dy^{III}$ is being predominantly $m_J = \pm 15/2$. The **g**-tensors of the ground state are estimated to be $g_x = 0.0222$, $g_y = 0.1163$, and $g_z = 19.6983$. Although the **g**-tensors are Ising, significant transverse


DOI: 10.1021/acs.inorgchem.7b02917
Inorg. Chem. 2018, 57, 3683−3698

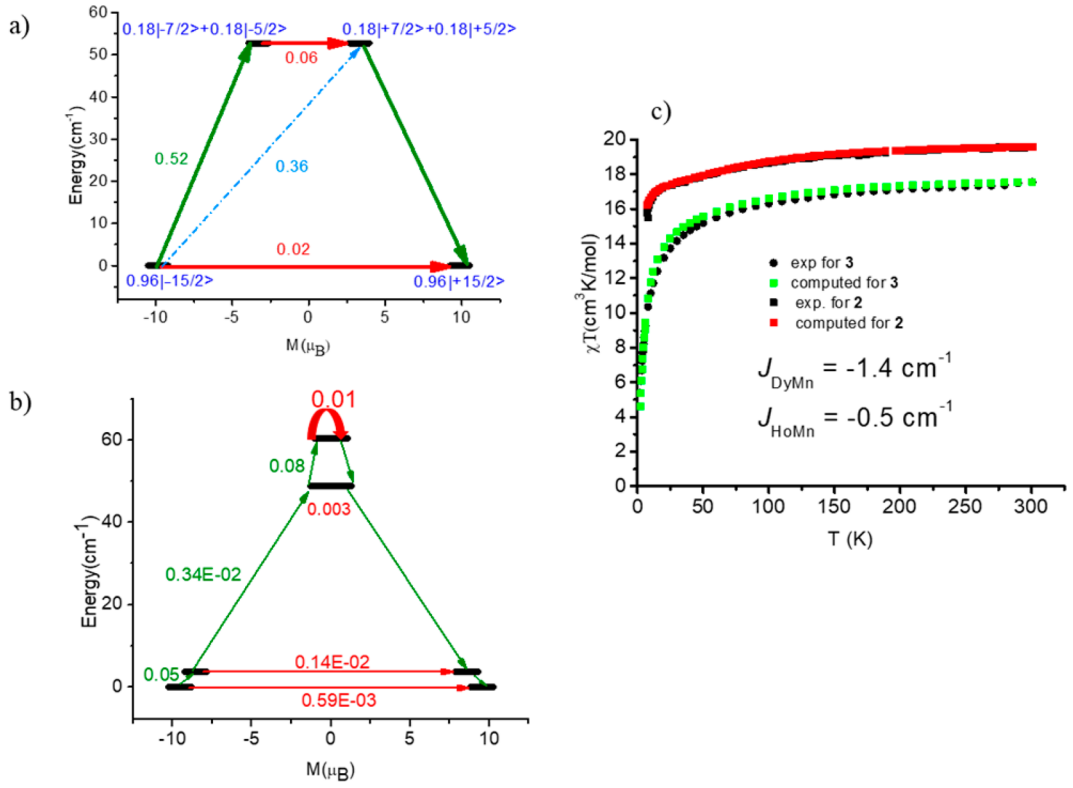


**Figure 15.** (a) Magnetization blocking barrier for the Dy site computed using *ab initio* calculations. The thick black line indicates the Kramers doublets (KDs) as a function of computed magnetic moment. The green/sky blue arrows show the possible pathway through Orbach/Raman relaxation. The red lines represent the presence of QTM/TA-QTM between the connecting pairs. The numbers provided at each arrow are the mean absolute value for the corresponding matrix element of the transition magnetic moment. (b) Mechanism of magnetic relaxation computed using POLY_ANISO for the coupled {$Mn^{III}Dy^{III}$} dinuclear system. (c) Temperature-dependent $\chi_M T$ plot for complexes **2** and **3**. For complex **2**, the red line corresponds to *ab initio* simulations ($J_{DyMn}$ = −1.40 $cm^{-1}$) and constant intermolecular interaction ($zJ$) of −0.004 $cm^{-1}$. For complex **3**, green lines correspond to *ab initio* simulations ($J_{HoMn}$ = −0.50 $cm^{-1}$) and constant intermolecular interaction ($zJ$) of 0.002 $cm^{-1}$.

anisotropy is detected at the ground state. The first excited state found to lie at 53 $cm^{-1}$, and the **g**-tensors of the first excited states are found to be $g_x$ = 0.1412, $g_y$ = 0.2008, $g_z$ = 18.7750, revealing again significant transverse anisotropy. The mechanism of magnetization relaxation that developed reveals significant QTM at the ground state and even higher probability at the exited state, rationalizing the absence of out-of-phase signals in the zero-field conditions. However, the computed tunnelling coefficients are relatively small and could be partially quenched in applied field conditions, and this may be attributed to the weak signals witnessed in the 1000 Oe data. In addition, the magnetic coupling between the {$Mn^{III}Dy^{III}$} could also help to quench the QTM to a certain extent. The Lines model fit to the susceptibility yield $J$ value of −1.4 $cm^{-1}$ (see Figure 15c), and this matches with the estimate obtained for the {MnGd} pair. The computed ground state orientations of the $Dy^{III}$ **g**-tensors are shown in Figure 6 along with the **D**-tensors computed for the $Mn^{III}$ ion. Clearly, the $g_{zz}$ and $D_{zz}$ are axes that are perpendicular to each other (title angle is 89.3°), and this noncoincidence of the anisotropic axes led to a reduction in the overall anisotropy and hence the absence of out-of-phase signals in the ac susceptibility data. The mechanism of magnetic relaxation developed for the dinuclear system is shown in Figure 15b. Although the magnetic exchange reduces the tunnelling at the ground state, the QTM is still high at the ground state level. Furthermore, the first excited state is found to lie at 3.6 $cm^{-1}$ with a large QTM probability, and the likely route for the relaxation under an applied field condition revealing why strong out-of-phase signals are absent for complex **2**.

In addition, we have also performed calculations on complex **3** for both single-ion $Ho^{III}$ and the {$Mn^{III}Ho^{III}$} dinuclear system. The single-ion calculations reveal the ground state $g_{zz}$ as 15.838, and this corresponds to $m_J$ = ±7 as revealed by the wave function analysis but mixed strongly with other lower $m_J$ levels. In addition, the ground state was found to have an exceedingly large tunnel splitting of 10.3 $cm^{-1}$, revealing a strong tunnelling between the ground $m_J$ levels. With POLY_ANISO and the Lines model yield, a $J$ value of −0.5 $cm^{-1}$ was extracted. The coupling is weak compared to the value obtained for the {$Mn^{III}Dy^{III}$} pair, revealing why this compound does not exhibit strong out-of-phase signals even in the presence of an applied field (see Figure 15c). The computed $g_{zz}$ orientations of the $Ho^{III}$ ion and the $Mn^{III}$ ion are also found to antagonize each other, leading to a reduction in the anisotropy and hence the absence of any SMM characteristics for this molecule (see Figure 6b). Although calculations are not performed for complex **4**, we believe that the magnetic characteristics are similar to those of **2** and **3**.

## CONCLUSIONS

We have first prepared strictly dinuclear $Mn^{III}/Ln^{III}$ complexes with an aminobis(phenol) ligand and thoroughly studied their structure and magnetic behavior by both experimental and computational methods. In these complexes, the $Mn^{III}$ ion exhibits a $MnN_2O_4$ distorted elongated octahedral coordination


DOI: 10.1021/acs.inorgchem.7b02917
Inorg. Chem. 2018, 57, 3683−3698

sphere, whereas the $Ln^{III}$ ions displays a distorted $LnO_9$ coordination environment. The metal ions are connected by double phenoxide/methoxide bridging groups. The $Mn^{III}Gd^{III}$ derivative was shown to exhibit weak antiferromagnetic interaction between the metal ions, with a negative axial zero-field splitting $D$ parameter. The sign and magnitude of $D$ were supported by *ab initio* calculations. DFT calculations show that the antiferromagnetic contribution to the exchange coupling between the $Mn^{III}$ and $Gd^{III}$ ions arises from the overlap between the single occupied magnetic orbitals (SOMO) of the $Mn^{III}$ ions with the 4f orbitals of the $Gd^{III}$ ion. In this case the overlap is particularly large because the $\sigma$-antibonding orbital of the OMe group is strongly overlapping with some of the 4f orbitals, and this in turn overlaps with $Mn^{III}$ $d_{xz}/d_{yz}$ orbitals. The ferromagnetic contribution to the exchange arises from orbital orthogonality between the SOMOs of $Mn^{III}$(3d) and $Gd^{III}$(4f) ions, as well as from a charge-transfer process from the 3d orbital to the formally empty 5d orbitals of $Gd^{III}$. The strong antiferromagnetic contribution overcomes the ferromagnetic one so that a net antiferromagnetic exchange is observed. Extensive magneto-structural correlations have been developed by varying the Mn−O−Gd angle and the Mn−O−Gd−O dihedral to understand the behavior of the $Mn^{III}$−$Gd^{III}$ interaction. The correlations indicate that Mn−O−Gd angles play a prominent role to govern the nature and magnitude of the magnetic exchange interaction. In this regard, $J$ values increase almost linearly with the Mn−O−Gd bond angle and become ferromagnetic for angle values higher than ∼107°. At lower Mn−O−Gd angles, $Mn^{III}$ and $Gd^{III}$ ions are closer to each other, and the overlap between the magnetic orbital augments, leading to an antiferromagnetic coupling. In contrast, at higher angles, the overlap between the SOMOs of $Mn^{III}$ and $Gd^{III}$ diminishes, leading to ferromagnetic coupling. Moreover, at large Mn−O−Gd angles, the charge-transfer contribution also enhances the ferromagnetic coupling. The spin densities on the metal ions suggest that $Mn^{III}$ provokes stronger delocalization (polarization) at higher angles, and this is correlated to the magnitude of the calculated exchange coupling constant and QTAIM results. The Mn−O−Gd−O dihedral angle has a lesser influence on $J$ compared to that of the Mn−O−Gd angle. When the Mn−O−Gd−O dihedral increases, the ferromagnetic contribution to the net exchange decreases until the dihedral angle reaches ∼11.15°; afterward, the contribution increases, leading to net ferromagnetic coupling. Therefore, a ferromagnetic {MnGd} interaction is predicted at both lower and higher dihedral angles. All these findings are well-supported by the QTAIM analysis.

Finally, ac measurements indicate field-induced slow relaxation of the magnetization in the $Mn^{III}$−$Dy^{III}$ and $Mn^{III}$−$Er^{III}$ complexes but without reaching a maximum, probably because either the thermal energy barrier for the reorientation of the magnetization is very low and/or there exists a faster QTM relaxation process. These complexes represent another example of how the combination of two anisotropic metal ions does not guarantee SMM behavior. The small effective energy barrier ($U_{eff}$) in these complexes can be due to the nonfavorable orientation of the main local anisotropies axes of $Mn^{III}$ and $Ln^{III}$ ions leading to a relatively low anisotropy for the whole molecule and to the existence of weak antiferromagnetic coupling between $Mn^{III}$ and $Ln^{III}$ ions favoring fast QTM and quenching slow relaxation of magnetization.

*Ab initio* calculations performed on the $\{Mn^{III}Dy^{III}\}$ complex support the experimental observations and clearly reveal significant QTM effects in the ground state, and the $\{Mn^{III}Dy^{III}\}$ exchange is found to be antiferromagnetic but not strong enough to quench the tunnelling. In addition, both the $g_{zz}$ axis of the $Dy^{III}$ and the $D_{zz}$ axis of the $Mn^{III}$ ions are perpendicular to each other, leading to weaker anisotropy and faster relaxation. For the $\{Mn^{III}Ho^{III}\}$ complex, a large tunnel splitting and much weaker exchange are the origin of the absence of SMM characteristics.

## EXPERIMENTAL SECTION

**Materials and Instrumentation.** All starting materials were reagent grade, purchased from Sigma-Aldrich and used as received. Solvents were of HPLC grade and used without any additional drying. All syntheses were performed under ambient laboratory atmosphere. All $Ln(NO_3)_3{\cdot}6H_2O$ was synthesized by dissolving a slight excess of $Ln_2O_3$ in hot 50% (v/v) nitric acid. Undissolved oxide was removed by decantation, and the solution was concentrated by heating. The $Ln(NO_3)_3{\cdot}6H_2O$ was precipitated from the solution during the cooling, in the refrigerator. Ligand $H_2L$ was synthesized according to the literature.[14] Elemental analysis was performed by using a Vario El III elemental analyzer. Single-crystal X-ray measurements were performed by using an Enraf Nonius Kappa CCD area detector diffractometer with the use of graphite monochromated Mo K$\alpha$ radiation. Variable-temperature (2−300 K) magnetic susceptibility measurements on polycrystalline samples were carried out with a Quantum Design Squid MPMSXL-5 device operating at 0.1 T from room temperature to 2 K. The experimental susceptibilities were corrected for the diamagnetism of the constituent atoms by using Pascal's tables. Alternating current experiments were performed using an oscillating ac field of 3.5 Oe and frequencies ranging from 1 to 1500 Hz.

**General Procedure for Synthesis of 1−4.** A 0.2 mmol (51 mg) portion of $Mn(NO_3)_2{\cdot}4H_2O$ and 0.2 mmol (97 mg) of ligand $H_2L$ were dissolved in 18 mL of methanol. To the intense brown/green solution was added 0.4 mmol (56 $\mu$L) of triethylamine and 0.2 mmol of $Ln(NO_3)_3{\cdot}xH_2O$. The crystallization had already started within about 30 min, but the solutions were left to crystallize overnight. The dark green crystals were separated by filtration and washed with diethyl ether. For **1**, yield was 130 mg (66% based on Mn). Anal. Calcd for $C_{31}H_{45}GdMnN_5O_{17}$ (974.16): C 38.23, H 4.86, N 7.19. Found: C 38.39, H 4.91, N 7.16. For **2**, the yield was 100 mg (51% based on Mn). Anal. Calcd. for for $C_{31}H_{47}DyMnN_5O_{17}$ (979.17): C 38.03, H 4.84, N 7.15. Found: C 38.11, H 4.89, N 6.94. For **3**, the yield was 120 mg (61% based on Mn). Anal. Calcd for $C_{31}H_{47}HoMnN_5O_{17}$ (981.60): C 37.93, H 4.83, N 7.13. Found: C 37.92, H 4.86, N 6.87. For **4**, the yield was 110 mg (58% based on Mn). Anal. Calcd for $C_{31}H_{47}ErMnN_5O_{17}$ (983.93): C 37.84, H 4.81, N 7.12. Found: C 37.89, H 4.78, N 6.98.

**Details of the Crystallographic Structure Determination.** Additional information from the data collection and refinement of compounds **1**−**4** is summarized in Table S8. The crystallographic data for **1**, **3**, and **4** were collected at 123 K with an Enraf Nonius Kappa CCD area-detector diffractometer with the use of graphite-monochromated Mo K$\alpha$ radiation ($\lambda$ = 0.71073 Å). Data collection was performed by using $\varphi$ and $\omega$ scans, and the data were processed by using DENZO-SMN v0.93.0.[33] SADABS[34] absorption correction was applied for compounds. The structures were solved by direct methods by using the SHELXS-97[35] or SIR-97[36] program, and the full-matrix least-squares refinements on $F^2$ were performed using the SHELXL-97[35] program. Figures were drawn with Diamond 3.[37] For all compounds the heavy atoms were refined anisotropically. The CH hydrogen atoms were included at the calculated distances with fixed displacement parameters from their host atoms (1.2 or 1.5 times of the host atom). The OH hydrogens were located from the electron density map and refined isotropically.

**Computational Details.** All calculations were carried out with the Gaussian09 program package[38] using the UB3LYP functional[39] with the double-$\zeta$ quality basis set employing CRENBL ECP relativistic effective core potential on Gd atom and Ahlrichs TZV basis set for the


DOI: 10.1021/acs.inorgchem.7b02917
Inorg. Chem. 2018, 57, 3683−3698

rest of the atoms. The DFT calculations combined with the Broken Symmetry (BS) approach have been employed to estimate the exchange constant between the $Mn^{III}$–$Gd^{III}$ ions. The simulation of magnetic susceptibility data is obtained using PHI software.[15] A quadratic convergence method was employed to determine the more stable wave functions in the SCF process. We have previously established a computational approach for reliably computing exchange coupling constants in 3d/4f complexes using broken-symmetry DFT, and this methodology has been employed here.[40−46]The all-electron calculations have been performed using the Douglas−Kroll−Hess (DKH) method to include the relativistic effect. The $\langle S^2\rangle_{HS}$ and $\langle S^2\rangle_{BS}$ values for different functional and basis sets are given in Tables 2 and 3. The wave functions for quantum theory of atoms in molecules (QTAIM) analysis were generated from single point calculations using the hybrid B3LYP functional[47−49] with a combination of CRENBL ECP on Gd and TZV Ahlrichs triple-ζ basis set on other atoms as implemented in the Gaussian 09 suite[38] of programs. In this study, QTAIM calculations are performed using AIM2000 package.[50] Computations of magnetic anisotropy of complexes **1** and **2** were carried out using post-Hartree−Fock *ab initio* calculations with the MOLCAS8.0 package.[19,20] We have followed the diamagnetic substitution method to calculate the anisotropy and magnetic relaxation. Gd(III), Dy(III), and Ho(III) were replaced by Lu(III) to estimate the zero-field parameter of Mn(III). Similarly, Mn(III) was replaced by Co(III) to calculate magnetic anisotropy of Gd(III) and Dy(III) in complexes **1** and **2**, respectively. Wave functions for complexes **1** and **2** were generated by CASSCF and RASSCF level of theory implemented in MOLCAS8.0 code. The Douglas−Kroll−Hess Hamiltonian was used to take into account the scalar relativistic effects in two steps. The Cholesky decomposition technique was used, and this reduces the computational cost of two electron integrals.[51] Since a relativistic Hamiltonian is used with relativistic basis sets to avoid the convergence problem, we have used basis sets of atomic natural type with relativistic core corrections. The basis set with triple-ζ plus polarization quality (VTZP) for $Mn^{III}$, $Gd^{III}$, and $Dy^{III}$ and double-ζ plus polarization (VDZP) atoms of the ligand (O, N) that resides in the first coordination sphere around metal ions was employed throughout our study. A basis set with double-ζ (VDZ) quality was used for the rest of the atoms. All the basis sets were taken from the ANO-RCC library implemented in the MOLCAS8.0 package.[18,19] At first, the CASSCF calculation was performed for all the complexes with 4 electrons in 5 active d orbitals CAS(4, 5) for Mn(III), 7 electrons in 7 f orbitals CAS(7,7) for Gd(III), and 9 electrons in 7 f orbitals CAS(9,7) for Dy(III). There were 5 quintets and 45 triplet states for Mn(III), 1 octet for Gd(III), and 21 sextet states for Dy(III) considered in the active space of our study. In the case of Ho, 35 quintets and 210 triplet states were considered. Then spin−orbit-free states were generated by the RASSCF method that include only a few CSFs and are defined in such way that avoids the inclusion of the higher-energy states. Spin−orbit interaction between spin-free states has been taken into account by RASSI-SO methodology. The magnetic susceptibility, **g**-tensors, barrier height, and quantum tunnelling were computed by SINGLE-ANISO code,[52] that uses the energies and magnetic moment of all spin−orbit states calculated from the RASSI step. The Lines model implemented within the POLY_ANISO program[32] has been used to calculate and obtain magnetic exchange between $Mn^{III}$ and $Dy^{III}$ ions. Detailed methodology for obtaining these parameters is described elsewhere.[10c,d]

## ■ ASSOCIATED CONTENT

### Supporting Information

The Supporting Information is available free of charge on the ACS Publications website at DOI: 10.1021/acs.inorgchem.7b02917.

X-ray crystallographic data, and additional computational and magnetic data (PDF)

### Accession Codes

CCDC 1585387−1585390 contain the supplementary crystallographic data for this paper. These data can be obtained free of charge via www.ccdc.cam.ac.uk/data_request/cif, or by emailing data_request@ccdc.cam.ac.uk, or by contacting The Cambridge Crystallographic Data Centre, 12 Union Road, Cambridge CB2 1EZ, UK; fax: +44 1223 336033.

## ■ AUTHOR INFORMATION


### Corresponding Authors

*E-mail: mikko.m.hanninen@jyu.fi.
*E-mail: rajaraman@chem.iitb.ac.in.
*E-mail: ecolacio@ugr.es.

### ORCID

Mikko M. Hänninen: 0000-0002-8380-7875


### Notes

The authors declare no competing financial interest.

## ■ ACKNOWLEDGMENTS

Financial support from the University of Jyväskylä and the Academy of Finland (M.M.H., Grant 274505) is greatly appreciated. E.C. and A. J. M. are grateful to the Ministerio de Economía y Competitividad (MINECO) and EU Feder Funds (Project CTQ2014-56312-P), the Junta de Andalucía (FQM-195 and the Project of Excellence P11-FQM-7756) and the University of Granada for financial support. G.R. would like to thank SERB (EMR/2014/00024), INSA, for financial support.

## ■ REFERENCES


(1) (a) Ward, M. D. Transition-metal sensitised near-infrared luminescence from lanthanides in d−f heteronuclear arrays. *Coord. Chem. Rev.* **2007**, *251*, 1663−1677. (b) Binnemans, K. Lanthanide-Based Luminescent Hybrid Materials. *Chem. Rev.* **2009**, *109*, 4283−4374. (c) Bünzli, J.-C. G. Benefiting from the Unique Properties of Lanthanide Ions. *Acc. Chem. Res.* **2006**, *39*, 53−61.

(2) (a) Deng, H.; Chun, S.; Florian, P.; Grandinetti, P. J.; Shore, S. G. Direct Lanthanide−Transition Metal Interactions: Synthesis of $(NH_3)_2YbFe(CO)_4$ and Crystal Structures of $\{[(CH_3CN)_3YbFe(CO)_4]2{\cdot}CH_3CN\}_\infty$ and $[(CH_3CN)_3YbFe(CO)_4]_\infty$. *Inorg. Chem.* **1996**, *35*, 3891−3896. (b) Evangelisti, F.; More, R.; Hodel, F.; Luber, S.; Patzke, G. R. 3d−4f $\{Co^{II}_3Ln(OR)_4\}$ Cubanes as Bio-Inspired Water Oxidation Catalysts. *J. Am. Chem. Soc.* **2015**, *137*, 11076−11084.

(3) (a) Winpenny, R. E. P. The structures and magnetic properties of complexes containing 3d- and 4f-metals. *Chem. Soc. Rev.* **1998**, *27*, 447−452. (b) Sakamoto, M.; Manseki, K.; Okawa, H. d−f Heteronuclear complexes: synthesis, structures and physicochemical aspects. *Coord. Chem. Rev.* **2001**, *219*, 379−414. (c) Huang, Y.-G.; Jiang, F.-L.; Hong, M.-C. Magnetic lanthanide−transition-metal organic−inorganic hybrid materials: From discrete clusters to extended frameworks. *Coord. Chem. Rev.* **2009**, *253*, 2814−2834. (d) Benelli, C.; Gatteschi, D. Magnetism of Lanthanides in Molecular Materials with Transition-Metal Ions and Organic Radicals. *Chem. Rev.* **2002**, *102*, 2369−2388. (e) Sessoli, R.; Powell, A. K. Strategies towards single molecule magnets based on lanthanide ions. *Coord. Chem. Rev.* **2009**, *253*, 2328−2341. (f) Andruh, M.; Costes, J. P.; Diaz, C.; Gao, S. 3d−4f Combined Chemistry: Synthetic Strategies and Magnetic Properties. *Inorg. Chem.* **2009**, *48*, 3342−3359. (g) Brechin, E. K., Ed. Molecular Magnets themed issue. *Dalton Trans.* **2010**, *39*, 4653−5040. (h) Sharples, J. W.; Collison, D. The coordination chemistry and magnetism of some 3d−4f and 4f amino-polyalcohol compounds. *Coord. Chem. Rev.* **2014**, *260*, 1−20. (i) Zheng, Y.-Z.; Zhou, G.-J.; Zheng, Z.; Winpenny, R. E. P. *Chem. Soc. Rev.* **2014**, *43*, 1462−1475. (j) Rosado Piquer, L.; Sañudo, E. C. Heterometallic 3d−




DOI: 10.1021/acs.inorgchem.7b02917
*Inorg. Chem.* 2018, 57, 3683−3698

4f single-molecule magnets. *Dalton Trans.* **2015**, *44*, 8771−8780. (k) Chow, C. Y.; Trivedi, E. R.; Pecoraro, V.; Zaleski, C. M. Heterometallic Mixed *3d-4f* Metallacrowns: Structural Versatility, Luminescence, and Molecular Magnetism. *Comments Inorg. Chem.* **2015**, *35*, 214−253. (l) Liu, K.; Shi, W.; Cheng, P. Toward heterometallic single-molecule magnets: Synthetic strategy, structures and properties of 3d−4f discrete complexes. *Coord. Chem. Rev.* **2015**, *289*−*290*, 74−122. (m) Polyzou, C. D.; Efthymiou, C. G.; Escuer, A.; Cunha-Silva, L.; Papatriantafyllopoulou, C.; Perlepes, S. P. In search of 3d/4f-metal single-molecule magnets: Nickel(II)/lanthanide(III) coordination clusters. *Pure Appl. Chem.* **2013**, *85*, 315−327.

(4) (a) Rinehart, J. D.; Long, J. R. Exploiting single-ion anisotropy in the design of f-element single-molecule magnets. *Chem. Sci.* **2011**, *2*, 2078−2085. (b) Wang, B. W.; Gao, S. In *The Rare Earth Elements, Fundamental and Applications*; Atwood, D. A., Ed.; John Wiley and Sons, 2012.

(5) (a) Gatteschi, D.; Sessoli, R.; Villain, J. *Molecular Nanomagnets*; Oxford University Press: Oxford, 2006. (b) *Molecular Magnets: Physics and Applications*; Bartolomé, J., Luis, F., Fernández, J. F., Eds.; Springer-Verlag: Berlin, 2014. (c) *Molecular Nanomagnets and Related Phenomena*; Gao, S., Ed.; Structure and Bonding (Berlin); Springer-Verlag: Berlin, 2015; Vol. *164*.

(6) Some reviews: (a) Evangelisti, M.; Brechin, E. K. Recipes for enhanced molecular cooling. *Dalton Trans.* **2010**, *39*, 4672−4676. (b) Sharples, J. W.; Collison, D. Coordination compounds and the magnetocaloric effect. *Polyhedron* **2013**, *66*, 15−27. (c) Sessoli, R. Chilling with Magnetic Molecules. *Angew. Chem., Int. Ed.* **2012**, *51*, 43−45. (d) Luis, F.; Evangelisti, M. In *Molecular Nanomagnet and Related Phenomena*; Gao, S., Ed.; Springer-Verlag: Berlin, Germany, 2014; pp 431−460. (e) Evangelisti, M. In *Molecular Magnets: Physics and Applications*; Bartolomé, J., Luis, F., Fernández, J., Eds.; Springer-Verlag: Berlin, Germany, 2014; pp 365−385. (f) Liu, J.-L.; Chen, Y.-C.; Guo, F.-S.; Tong, M.-L. Recent advances in the design of magnetic molecules for use as cryogenic magnetic coolants. *Coord. Chem. Rev.* **2014**, *281*, 26−49. (g) Zhang, S.; Cheng, P. Coordination-Cluster-Based Molecular Magnetic Refrigerants. *Chem. Rec.* **2016**, *16*, 2077−2126.

(7) (a) Bogani, L.; Wernsdorfer, W. Molecular spintronics using single-molecule magnets. *Nat. Mater.* **2008**, *7*, 179−186. (b) Vincent, R.; Klyatskaya, S.; Ruben, M.; Wernsdorfer, W.; Balestro, F. Electronic read-out of a single nuclear spin using a molecular spin transistor. *Nature* **2012**, *488*, 357−360. (c) Ganzhorn, M.; Klyatskaya, S.; Ruben, M.; Wernsdorfer, W. Strong spin−phonon coupling between a single-molecule magnet and a carbon nanotube nanoelectromechanical system. *Nat. Nanotechnol.* **2013**, *8*, 165−169. (d) Jenkins, M.; Hümmer, T.; Martínez-Pérez, M. J.; García-Ripoll, J.; Zueco, D.; Luis, F. Coupling single-molecule magnets to quantum circuits. *New J. Phys.* **2013**, *15*, 095007. (e) Prezioso, M.; Riminucci, A.; Graziosi, P.; Bergenti, I.; Rakshit, R.; Cecchini, R.; Vianelli, A.; Borgatti, F.; Haag, N.; Willis, M.; Drew, A. J.; Gillin, W. P.; Dediu, V. A. A Single-Device Universal Logic Gate Based on a Magnetically Enhanced Memristor. *Adv. Mater.* **2013**, *25*, 534−538. (f) Mannini, M.; Pineider, F.; Danieli, C.; Totti, F.; Sorace, L.; Sainctavit, Ph.; Arrio, M. A.; Otero, E.; Joly, L.; Cezar, J. C.; Cornia, A.; Sessoli, R. Quantum tunnelling of the magnetization in a monolayer of oriented single-molecule magnets. *Nature* **2010**, *468*, 417−421. (g) Thiele, S.; Balestro, F.; Ballou, R.; Klyatskaya, S.; Ruben, M.; Wernsdorfer, W. Electrically driven nuclear spin resonance in single-molecule magnets. *Science* **2014**, *344*, 1135−1138. (h) Cornia, A.; Seneor, P. Spintronics: The molecular way. *Nat. Mater.* **2017**, *16*, 505−506. (i) Lumetti, S.; Candini, A.; Godfrin, C.; Balestro, F.; Wernsdorfer, W.; Klyatskaya, S.; Ruben, M.; Affronte, M. Single-molecule devices with graphene electrodes. *Dalton Trans.* **2016**, *45*, 16570−16574.

(8) (a) Rocha, A. R.; García-Suárez, V. M.; Bailey, S. W.; Lambert, C. J.; Ferrer, J.; Sanvito, S. Towards Molecular Spintronics. *Nat. Mater.* **2005**, *4*, 335−339. (b) Affronte, M. Molecular Nanomagnets for Information Technologies. *J. Mater. Chem.* **2009**, *19*, 1731−1737.

(9) (a) Leuenberger, M. N.; Loss, D. Quantum computing in molecular magnets. *Nature* **2001**, *410*, 789−793. (b) Ardavan, A.; Rival, O.; Morton, J. J. L.; Blundell, S. J.; Tyryshkin, A. M.; Timco, G. A.; Winpenny, R. E. P. Will Spin-Relaxation Times in Molecular Magnets Permit Quantum Information Processing? *Phys. Rev. Lett.* **2007**, *98*, 057201. (c) Stamp, P. C. E.; Gaita-Ariño, A. Spin-based quantum computers made by chemistry: hows and whys. *J. Mater. Chem.* **2009**, *19*, 1718−1730. (d) Martínez-Pérez, M. J.; Cardona-Serra, S.; Schlegel, C.; Moro, F.; Alonso, P. J.; Prima-García, H.; Clemente-Juan, J. M.; Evangelisti, M.; Gaita-Ariño, A.; Sesé, J.; Van Slageren, J.; Coronado, E.; Luis, F. Gd-Based Single-Ion Magnets with Tunable Magnetic Anisotropy: Molecular Design of Spin Qubits. *Phys. Rev. Lett.* **2012**, *108*, 247213. (e) Ghirri, A.; Candini, A.; Affronte, M. Molecular Spins in the Context of Quantum Technologies. *Magnetochemistry* **2017**, *3* (1), 12.

(10) (a) Vignesh, K. R.; Langley, S. K.; Murray, K. S.; Rajaraman, G. Quenching the Quantum Tunneling of Magnetization in Heterometallic Octanuclear $\{TM^{III}_4Dy^{III}_4\}$ (TM = Co and Cr) Single-Molecule Magnets by Modification of the Bridging Ligands and Enhancing the Magnetic Exchange Coupling. *Chem. - Eur. J.* **2017**, *23*, 1654−1666. (b) Langley, S. K.; Wielechowski, D. P.; Moubaraki, B.; Murray, K. S. Enhancing the magnetic blocking temperature and magnetic coercivity of $\{Cr^{III}_2\ Ln^{III}_2\}$ single-molecule magnets via bridging ligand modification. *Chem. Commun.* **2016**, *52*, 10976−10979. (c) Gupta, T.; Beg, M. F.; Rajaraman, G. Role of Single-Ion Anisotropy and Magnetic Exchange Interactions in Suppressing Zero-Field Tunnelling in {3d-4f} Single Molecule Magnets. *Inorg. Chem.* **2016**, *55*, 11201−11215. (d) Singh, S. K.; Beg, M. F.; Rajaraman, G. Role of Magnetic Exchange Interactions in the Magnetization Relaxation of {3d−4f} Single-Molecule Magnets: A Theoretical Perspective. *Chem. - Eur. J.* **2016**, *22*, 672−680. (e) Li, X.-L.; Min, F.-Y.; Wang, C.; Lin, S.-Y.; Liu, Z.; Tang, J. Utilizing 3d−4f Magnetic Interaction to Slow the Magnetic Relaxation of Heterometallic Complexes. *Inorg. Chem.* **2015**, *54*, 4337−4344. (f) Langley, S. K.; Le, C.; Ungur, L.; Moubaraki, B.; Abrahams, B. F.; Chibotaru, L. F.; Murray, K. S. Heterometallic 3d−4f Single-Molecule Magnets: Ligand and Metal Ion Influences on the Magnetic Relaxation. *Inorg. Chem.* **2015**, *54*, 3631. (g) Xie, Q.-W.; Wu, S.-Q.; Shi, W.-B.; Liu, C.-M.; Cui, A.-L.; Kou, H.-Z. Heterodinuclear MII−LnIII single molecule magnets constructed from exchange-coupled single ion magnets. *Dalton Trans.* **2014**, *43*, 11309−11316.

(11) Langley, S. K.; Wielechowski, D. P.; Vieru, V.; Chilton, N. F.; Moubaraki, B.; Abrahams, B. F.; Chibotaru, L. F.; Murray, K. S. A $\{Cr^{III}_2Dy^{III}_2\}$ Single-Molecule Magnet: Enhancing the Blocking Temperature through 3d Magnetic Exchange. *Angew. Chem., Int. Ed.* **2013**, *52*, 12014−12019.

(12) (a) Rajaraman, G.; Totti, F.; Bencini, A.; Caneschi, A.; Sessoli, R.; Gatteschi, D. Density functional studies on the exchange interaction of a dinuclear Gd(III)−Cu(II) complex: method assessment, magnetic coupling mechanism and magneto-structural correlations. *Dalton Trans.* **2009**, 3153−3161. (b) Singh, S. K.; Pedersen, K. S.; Sigrist, M.; Thuesen, C. A.; Schau-Magnussen, M.; Mutka, H.; Piligkos, S.; Weihe, H.; Rajaraman, G.; Bendix, J. Angular dependence of the exchange interaction in fluoride-bridged GdIII−CrIII complexes. *Chem. Commun.* **2013**, *49*, 5583−5585. (c) Singh, S. K.; Rajaraman, G. *Dalton Trans.* **2013**, *42*, 3623. (d) Cremades, E.; Gomez-Coca, S.; Aravena, D.; Alvarez, S.; Ruiz, E. Theoretical Study of Exchange Coupling in 3d-Gd Complexes: Large Magnetocaloric Effect Systems. *J. Am. Chem. Soc.* **2012**, *134*, 10532−10542. (e) Colacio, E.; Ruiz, J.; Mota, A. J.; Palacios, M. A.; Cremades, E.; Ruiz, E.; White, F. J.; Brechin, E. K. Family of Carboxylate- and Nitrate-diphenoxo Triply Bridged Dinuclear NiIILnIII Complexes (Ln = Eu, Gd, Tb, Ho, Er, Y): Synthesis, Experimental and Theoretical Magneto-Structural Studies, and Single-Molecule Magnet Behavior. *Inorg. Chem.* **2012**, *51*, 5857−5868. (f) Paulovic, J.; Cimpoesu, F.; Ferbinteanu, M.; Hirao, K. Mechanism of Ferromagnetic Coupling in Copper(II)-Gadolinium(III) Complexes. *J. Am. Chem. Soc.* **2004**, *126*, 3321−3331. (g) Ferbinteanu, M.; Stroppa, A.; Scarrozza, M.; Humelnicu, I.; Maftei, D.; Frecus, B.; Cimpoesu, F. On The Density Functional Theory Treatment of Lanthanide Coordination Compounds: A



DOI: 10.1021/acs.inorgchem.7b02917
*Inorg. Chem.* 2018, 57, 3683−3698

Comparative Study in a Series of Cu−Ln (Ln = Gd, Tb, Lu) Binuclear Complexes. *Inorg. Chem.* **2017**, *56*, 9474−9485.
(13) Some examples: (a) Ako, A. M.; Mereacre, V.; Clérac, R.; Wernsdorfer, W.; Hewitt, I. J.; Anson, C. E.; Powell, A. K. A $[Mn_{18}Dy]$ SMM resulting from the targeted replacement of the central $Mn^{II}$ in the S = 83/2 $[Mn_{19}]$-aggregate with $Dy^{III}$. *Chem. Commun.* **2009**, 544−546. (b) Karotsis, G.; Kennedy, S.; Teat, S. J.; Beavers, C. M.; Fowler, D. A.; Morales, J. J.; Evangelisti, M.; Dalgarno, S. J.; Brechin, E. K. $[Mn^{III}_4Ln^{III}_4]$ Calix[4]arene Clusters as Enhanced Magnetic Coolers and Molecular Magnets. *J. Am. Chem. Soc.* **2010**, *132*, 12983−12990. (c) Li, M.; Ako, A. M.; Lan, Y.; Wernsdorfer, W.; Buth, G.; Anson, C. E.; Powell, A. K.; Wang, Z.; Gao, S. New heterometallic [MnIII4LnIII4] wheels incorporating formate ligands. *Dalton Trans.* **2010**, *39*, 3375−3377. (d) Li, M.; Lan, Y.; Ako, A. M.; Wernsdorfer, W.; Anson, C. E.; Buth, G.; Powell, A. K.; Wang, Z.; Gao, S. A Family of 3d-4f Octa-Nuclear $[Mn^{III}_4Ln^{III}_4]$ Wheels (Ln = Sm, Gd, Tb, Dy, Ho, Er, and Y): Synthesis, Structure, and Magnetism. *Inorg. Chem.* **2010**, *49*, 11587−11594. (e) Mukherjee, S.; Daniels, M. R.; Bagai, R.; Abboud, K. A.; Christou, G.; Lampropoulos, C. A variety of new tri- and tetranuclear Mn−Ln and Fe−Ln (Ln = lanthanide) complexes. *Polyhedron* **2010**, *29*, 54−65. (f) Mereacre, V.; Lan, Y.; Clérac, R.; Ako, A. M.; Hewitt, I. J.; Wernsdorfer, W.; Buth, G.; Anson, C. E.; Powell, A. K. Family of $Mn^{III}_2Ln_2(\mu_4\text{-O})$ Compounds: Syntheses, Structures, and Magnetic Properties. *Inorg. Chem.* **2010**, *49*, 5293−5302. (g) Yang, P. P.; Wang, X. L.; Liao, D. Z.; Li, L.-C. Synthesis, structure and magnetic properties of a novel family of heterometallic nonanuclear $Na^{I}_2Mn^{III}_6Ln^{III}$ (Ln = Eu, Gd, Tb, Dy) complexes. *Dalton Trans.* **2011**, *40*, 4155−4161. (h) Rigaux, G.; Inglis, R.; Morrison, S.; Prescimone, A.; Cadiou, C.; Evangelisti, M.; Brechin, E. K. Enhancing $U_{eff}$ in oxime-bridged $[Mn^{III}_6Ln^{III}_2]$ hexagonal prisms. *Dalton Trans.* **2011**, *40*, 4797−4799. (i) Chesman, A. S. R.; Turner, D. R.; Berry, K. J.; Chilton, N. F.; Moubaraki, B.; Murray, K. S.; Deacon, G. B.; Batten, S. R. $Ln^{III}_2Mn^{III}_2$ heterobimetallic "butterfly" complexes displaying antiferromagnetic coupling (Ln = Eu, Gd, Tb, Er). *Dalton Trans.* **2012**, *41*, 11402−11412. (j) Xie, Q. W.; Cui, A. L.; Tao, J.; Kou, H. Z. Syntheses, structure, and magnetic properties of hexanuclear $Mn^{III}_2M^{III}_4$ (M = Y, Gd, Tb, Dy) complexes. *Dalton Trans.* **2012**, *41*, 10589−10595. (k) Papatriantafyllopoulou, C.; Abboud, K. A.; Christou, G. Carboxylate-Free $Mn^{III}_2Ln^{III}_2$ (Ln = Lanthanide) and $Mn^{III}_2Y^{III}_2$ Complexes from the Use of (2-Hydroxymethyl)pyridine: Analysis of Spin Frustration Effects. *Inorg. Chem.* **2011**, *50*, 8959−8966. (l) Zheng, Y.; Kong, X. J.; Long, L. S.; Huang, R. B.; Zheng, L. S. Enantiopure sandwich-type nonanuclear $Ln^{III}_3Mn^{III}_6$ clusters. *Dalton Trans.* **2011**, *40*, 4035−4037. (m) Tong, Y.-Z.; Wang, Q.-L.; Zhang, A.-P.; Ma, Y.; Yan, S.-P.; Yang, G.-M.; Cheng, P.; Liao, D.-Z. Crystal structure and magnetism of two new 3d−4f complexes contain Mn(III) and Ln(III) (Ln = Dy, Tb) ions. *Inorg. Chem. Commun.* **2013**, *32*, 32−36. (n) Langley, S. K.; Moubaraki, B.; Murray, K. S. Heterometallic Tetranuclear $\{Mn^{III}_2Ln^{III}_2\}_n$ 1D Coordination Polymers: Employing Sulfonate Ligands as Connecting Groups. *Aust. J. Chem.* **2014**, *67*, 1601−1606. (o) Vignesh, K. R.; Langley, S. K.; Moubaraki, B.; Murray, K. S.; Rajaraman, G. Large Hexadecametallic {MnIII−LnIII} Wheels: Synthesis, Structural, Magnetic, and Theoretical Characterization. *Chem. - Eur. J.* **2015**, *21*, 16364−16369. (p) Costes, J. P.; Tuchagues, J. P.; Vendier, L.; García-Tojal, J. A Strictly Dinuclear MnIII−GdIII Complex: Synthesis and Magnetic Properties. *Eur. J. Inorg. Chem.* **2013**, *2013*, 3307−3311.
(14) Hänninen, M. M.; Välivaara, J.; Mota, A. J.; Colacio, E.; Lloret, F.; Sillanpää, R. Ferromagnetic Dinuclear Mixed-Valence Mn(II)/Mn(III) Complexes: Building Blocks for the Higher Nuclearity Complexes. Structure, Magnetic Properties, and Density Functional Theory Calculations. *Inorg. Chem.* **2013**, *52*, 2228−2241.
(15) Chilton, N. F.; Anderson, R. P.; Turner, L. D.; Soncini, A.; Murray, K. S. PHI: A powerful new program for the analysis of anisotropic monomeric and exchange-coupled polynuclear d- and f-block complexes. *J. Comput. Chem.* **2013**, *34*, 1164−1175.
(16) Karotsis, G.; Evangelisti, M.; Dalgarno, S. J.; Brechin, E. K. A Calix[4]arene 3d/4f Magnetic Cooler. *Angew. Chem., Int. Ed.* **2009**, *48*, 9928−993−1.
(17) Liu, J.-L.; Lin, W.-Q.; Chen, Y.-C.; Leng, J.-D.; Guo, F.-S.; Tong, M.-L. Symmetry-Related $[Ln^{III}_6Mn^{III}_{12}]$ Clusters toward Single-Molecule Magnets and Cryogenic Magnetic Refrigerants. *Inorg. Chem.* **2013**, *52*, 457−463.
(18) (a) Aquilante, F.; Autschbach, J.; Carlson, R. K.; Chibotaru, L. F.; Delcey, M. G.; De Vico, L.; Fdez. Galván, I.; Ferré, N.; Frutos, L. M.; Gagliardi, L.; Garavelli, M.; Giussani, A.; Hoyer, C. E.; Li Manni, G.; Lischka, H.; Ma, D.; Malmqvist, P. Å.; Müller, T.; Nenov, A.; Olivucci, M.; Pedersen, T. B.; Peng, D.; Plasser, F.; Pritchard, B.; Reiher, M.; Rivalta, I.; Schapiro, I.; Segarra-Martí, J.; Stenrup, M.; Truhlar, D. G.; Ungur, L.; Valentini, A.; Vancoillie, S.; Veryazov, V.; Vysotskiy, V. P.; Weingart, O.; Zapata, F.; Lindh, R. Molcas 8: New capabilities for multiconfigurational quantum chemical calculations across the periodic table. *J. Comput. Chem.* **2016**, *37*, 506−541. (b) Aquilante, F.; De Vico, L.; Ferre, N.; Ghigo, G.; Malmqvist, P. A.; Neogrady, P.; Pedersen, T. B.; Pitonak, M.; Reiher, M.; Roos, B. O.; Serrano-Andres, L.; Urban, M.; Veryazov, V.; Lindh, R. MOLCAS 7: The Next Generation. *J. Comput. Chem.* **2010**, *31*, 224−247. (c) Duncan, J. A. MOLCAS 7.2. *J. Am. Chem. Soc.* **2009**, *131*, 2416−2417. (d) Veryazov, V.; Widmark, P. O.; Serrano-Andres, L.; Lindh, R.; Roos, B. O. 2MOLCAS as a development platform for quantum chemistry software. *Int. J. Quantum Chem.* **2004**, *100*, 626−635. (e) Karlstrom, G.; Lindh, R.; Malmqvist, P. A.; Roos, B. O.; Ryde, U.; Veryazov, V.; Widmark, P. O.; Cossi, M.; Schimmelpfennig, B.; Neogrady, P.; Seijo, L. MOLCAS: a program package for computational chemistry. *Comput. Mater. Sci.* **2003**, *28*, 222−239.
(19) Ungur, L.; Chibotaru, L. F. In *Lanthanides and Actinides in Molecular Magnetism*; Wiley-VCH Verlag GmbH & Co. KGaA, 2015; pp 153−184.
(20) (a) Gatteschi, D.; Sorace, L.; Sessoli, R.; Barra, A. L. High-frequency EPR: An occasion for revisiting ligand field theory. *Appl. Magn. Reson.* **2001**, *21*, 299−310. (b) Krzystek, J.; Telser, J. Measuring giant anisotropy in paramagnetic transition metal complexes with relevance to single-ion magnetism. *Dalton Trans.* **2016**, *45*, 16751−16763.
(21) (a) Singh, S. K.; Rajeshkumar, T.; Chandrasekhar, V.; Rajaraman, G. Theoretical studies on {3d-Gd} and {3d-Gd-3d} complexes: Effect of metal substitution on the effective exchange interaction. *Polyhedron* **2013**, *66*, 81−86. (b) Gupta, S. K.; Dar, A. A.; Rajeshkumar, T.; Kuppuswamy, S.; Langley, S. K.; Murray, K. S.; Rajaraman, G.; Murugavel, R. Discrete $\{Gd^{III}_4M\}$ (M = $Gd^{III}$ or $Co^{II}$) pentanuclear complexes: a new class of metal-organophosphate molecular coolers. *Dalton Trans.* **2015**, *44*, 5961−5965. (c) Gupta, T.; Rajeshkumar, T.; Rajaraman, G. Magnetic exchange in {$Gd^{III}$−radical} complexes: method assessment, mechanism of coupling and magneto-structural correlations. *Phys. Chem. Chem. Phys.* **2014**, *16*, 14568−14577. (d) Rajeshkumar, T.; Annadata, H. V.; Evangelisti, M.; Langley, S. K.; Chilton, N. F.; Murray, K. S.; Rajaraman, G. Theoretical Studies on Polynuclear $\{Cu^{II}_5Gd^{III}_n\}$ Clusters (n = 4, 2): Towards Understanding Their Large Magnetocaloric Effect. *Inorg. Chem.* **2015**, *54*, 1661−1670.
(22) Cundari, T. R.; Stevens, W. J. Effective core potential methods for the lanthanides. *J. Chem. Phys.* **1993**, *98*, 5555.
(23) Hurley, M.; Pacios, L. F.; Christiansen, P.; Ross, R.; Ermler, W. *Ab initio* relativistic effective potentials with spin-orbit operators. II. K through Kr. *J. Chem. Phys.* **1986**, *84*, 6840.
(24) Nakajima, T.; Hirao, K. Accurate relativistic Gaussian basis sets determined by the third-order Douglas−Kroll approximation with a finite-nucleus model. *J. Chem. Phys.* **2002**, *116*, 8270.
(25) Lenthe, E. V.; Baerends, E.-J.; Snijders, J. G. Relativistic regular two-component Hamiltonians. *J. Chem. Phys.* **1993**, *99*, 4597.
(26) Schäfer, A.; Huber, C.; Ahlrichs, R. Fully optimized contracted Gaussian basis sets of triple zeta valence quality for atoms Li to Kr. *J. Chem. Phys.* **1994**, *100*, 5829.
(27) Gupta, T.; Rajaraman, G. Modelling spin Hamiltonian parameters of molecular nanomagnets. *Chem. Commun.* **2016**, *52*, 8972−9008.
(28) Bader, R. F. *Atoms in Molecules—A Quantum Theory*; Oxford University Press: Oxford, U.K., 1990.


DOI: 10.1021/acs.inorgchem.7b02917
*Inorg. Chem.* 2018, 57, 3683−3698

(29) Bader, R. F. W. Bond Paths Are Not Chemical Bonds. *J. Phys. Chem. A* **2009**, *113*, 10391.
(30) Espinosa, E.; Alkorta, I.; Elguero, J.; Molins, E. From weak to strong interactions: A comprehensive analysis of the topological and energetic properties of the electron density distribution involving X−H···F−Y systems. *J. Chem. Phys.* **2002**, *117*, 5529.
(31) Jenkins, S.; Morrison, I. The chemical character of the intermolecular bonds of seven phases of ice as revealed by ab initio calculation of electron densities. *Chem. Phys. Lett.* **2000**, *317*, 97−102.
(32) (a) Chibotaru, L. F.; Ungur, L.; Soncini, A. Origin of non-magnetic Kramers doublets in the ground state of dysprosium triangles: Evidence for toroidal magnetic moment. *Angew. Chem., Int. Ed.* **2008**, *47*, 4126−4129. (b) Ungur, L.; Van den Heuvel, W.; Chibotaru, L. F. Ab initio investigation of non-collinear magnetic structure and lowest magnetic excitations in dysprosium triangles. *New J. Chem.* **2009**, *33*, 1224−1230. (c) Chibotaru, L. F.; Ungur, L.; Aronica, C.; Elmoll, H.; Pilet, G.; Luneau, D. Structure, magnetism and theoretical study of mixed-valent CoII3CoIII4 heptanuclear wheel: Lack of SMM behaviour despite negative magnetic anisotropy. *J. Am. Chem. Soc.* **2008**, *130*, 12445−12455.
(33) Otwinowski, Z.; Minor, W. *Methods in Enzymology: Part A*; Academic Press, New York, 1997.
(34) Sheldrick, G. M. *SADABS*; University of Göttingen: Göttingen, Germany, 2002.
(35) Sheldrick, G. M. A short history of SHELX. *Acta Crystallogr., Sect. A: Found. Crystallogr.* **2008**, *64*, 112−122.
(36) Altomare, A.; Burla, M. C.; Camalli, M.; Cascarano, G. L.; Giacovazzo, C.; Guagliardi, A.; Moliterni, A. G. G.; Polidori, G.; Spagna, R. SIR97: a new tool for crystal structure determination and refinement. *J. Appl. Crystallogr.* **1999**, *32*, 115−119.
(37) Brandenburg, K. *DIAMOND*; Crystal Impact GbR: Bonn, Germany, 1999.
(38) Frisch, M. J.; Trucks, G. W.; Schlegel, H. B.; Scuseria, G. E.; Robb, M. A.; Cheeseman, J. R.; Scalmani, G.; Barone, V.; Mennucci, B.; Petersson, G. A.; Nakatsuji, H.; Caricato, M.; Li, X.; Hratchian, H. P.; Izmaylov, A. F.; Bloino, J.; Zheng, G.; Sonnenberg, J. L.; Hada, M.; Ehara, M.; Toyota, K.; Fukuda, R.; Hasegawa, J.; Ishida, M.; Nakajima, T.; Honda, Y.; Kitao, O.; Nakai, H.; Vreven, T.; Montgomery, J. A., Jr.; Peralta, J. E.; Ogliaro, F.; Bearpark, M.; Heyd, J. J.; Brothers, E.; Kudin, K. N.; Staroverov, V. N.; Kobayashi, R.; Normand, J.; Raghavachari, K.; Rendell, A.; Burant, J. C.; Iyengar, S. S.; Tomasi, J.; Cossi, M.; Rega, N.; Millam, J. M.; Klene, M.; Knox, J. E.; Cross, J. B.; Bakken, V.; Adamo, C.; Jaramillo, J.; Gomperts, R.; Stratmann, R. E.; Yazyev, O.; Austin, A. J.; Cammi, R.; Pomelli, C.; Ochterski, J. W.; Martin, R. L.; Morokuma, K.; Zakrzewski, V. G.; Voth, G. A.; Salvador, P.; Dannenberg, J. J.; Dapprich, S.; Daniels, A. D.; Farkas, O.; Foresman, J. B.; Ortiz, J. V.; Cioslowski, J.; Fox, D. J. *GAUSSIAN 09*, Revision A.02; Gaussian, Inc.: Wallingford, CT, 2009.
(39) Becke, A. D. Density-functional thermochemistry. III. The role of exact exchange. *J. Chem. Phys.* **1993**, *98*, 5648.
(40) Singh, S. K.; Rajaraman, G. Decisive interactions that determine ferro/antiferromagnetic coupling in {3d−4f} pairs: a case study on dinuclear {V(IV)−Gd(III)} complexes. *Dalton Trans.* **2013**, *42*, 3623−3630.
(41) Rajaraman, G.; Totti, F.; Bencini, A.; Caneschi, A.; Sessoli, R.; Gatteschi, D. Density functional studies on the exchange interaction of a dinuclear Gd(III)−Cu(II) complex: method assessment, magnetic coupling mechanism and magneto-structural correlations. *Dalton Trans.* **2009**, 3153−3161.
(42) Singh, S. K.; Pedersen, K. S.; Sigrist, M.; Thuesen, C. A.; Schau-Magnussen, M.; Mutka, H.; Piligkos, S.; Weihe, H.; Rajaraman, G.; Bendix, J. Angular dependence of the exchange interaction in fluoride-bridged $Gd^{III}$−$Cr^{III}$ complexes. *Chem. Commun.* **2013**, *49*, 5583−5585.
(43) Singh, S. K.; Beg, M. F.; Rajaraman, G. Role of Magnetic Exchange Interactions in the Magnetization Relaxation of {3d−4f} Single-Molecule Magnets: A Theoretical Perspective. *Chem. - Eur. J.* **2016**, *22*, 672−680.
(44) Singh, S. K.; Rajeshkumar, T.; Chandrasekhar, V.; Rajaraman, G. Theoretical studies on {3d-Gd} and {3d-Gd-3d} complexes: Effect of metal substitution on the effective exchange interaction. *Polyhedron* **2013**, *66*, 81−86.
(45) Gupta, T.; Beg, M. F.; Rajaraman, G. Role of Single-Ion Anisotropy and Magnetic Exchange Interactions in Suppressing Zero-Field Tunnelling in {3d-4f} Single Molecule Magnets. *Inorg. Chem.* **2016**, *55*, 11201−11215.
(46) Singh, S. K.; Tibrewal, N. K.; Rajaraman, G. Density functional studies on dinuclear {$Ni^{II}Gd^{III}$} and trinuclear {$Ni^{II}Gd^{III}Ni^{II}$} complexes: magnetic exchange and magneto-structural maps. *Dalton Trans.* **2011**, *40*, 10897−10906.
(47) Lee, C.; Yang, W.; Parr, R. G. Development of the Colle-Salvetti correlation-energy formula into a functional of the electron density. *Phys. Rev. B: Condens. Matter Mater. Phys.* **1988**, *37*, 785−789.
(48) Stephens, P. J.; Devlin, F. J.; Chabalowski, C. F.; Frisch, M. J. *Ab Initio* Calculation of Vibrational Absorption and Circular Dichroism Spectra Using Density Functional Force Fields. *J. Phys. Chem.* **1994**, *98*, 11623−11627.
(49) Cundari, T. R.; Stevens, W. J. Effective core potential methods for the lanthanides. *J. Chem. Phys.* **1993**, *98*, 5555−5565.
(50) Biegler-König, F.; Schönbohm, J. Update of the AIM2000-Program for atoms in molecules. *J. Comput. Chem.* **2002**, *23*, 1489−1494.
(51) Koch, H.; Sánchez de Merás, A.; Pedersen, T. B. Reduced scaling in electronic structure calculations using Cholesky decompositions. *J. Chem. Phys.* **2003**, *118*, 9481−9484.
(52) (a) Langley, S. K.; Ungur, L.; Chilton, N. F.; Moubaraki, B.; Chibotaru, L. F.; Murray, K. S. Single-Molecule Magnetism in a Family of {$Co^{III}_2Dy^{III}_2$} Butterfly Complexes: Effects of Ligand Replacement on the Dynamics of Magnetic Relaxation. *Inorg. Chem.* **2014**, *53*, 4303−4315. (b) Habib, F.; Luca, O. R.; Vieru, V.; Shiddiq, M.; Korobkov, I.; Gorelsky, S. I.; Takase, M. K.; Chibotaru, L. F.; Hill, S.; Crabtree, R. H.; Murugesu, M. Influence of the Ligand Field on Slow Magnetization Relaxation versus Spin Crossover in Mononuclear Cobalt Complexes. *Angew. Chem., Int. Ed.* **2013**, *52*, 11290−11293. (c) Chibotaru, L. F.; Ungur, L. *Ab initio* calculation of anisotropic magnetic properties of complexes. I. Unique definition of pseudospin Hamiltonians and their derivation. *J. Chem. Phys.* **2012**, *137*, 064112−22.


DOI: 10.1021/acs.inorgchem.7b02917
*Inorg. Chem.* 2018, 57, 3683−3698